Evolution of a Terrestrial Multiple Moon System

Robin M. Canup and Harold F. Levison

Southwest Research Institute

and

Glen R. Stewart

Laboratory for Atmospheric and Space Physics

Received ____________________; accepted ____________________

Submitted to *Astronomical Journal*

ABSTRACT

The currently favored theory of lunar origin is the giant-impact hypothesis. Recent work that has modeled accretional growth in impact-generated disks (Ida, Canup and Stewart 1997) has found that systems with one or two large moons and external debris are common outcomes. In this paper we investigate the evolution of terrestrial multiple moon systems as they evolve due to mutual interactions (including mean-motion resonances) and tidal interaction with the Earth, using both analytical techniques and numerical integrations. We find that multiple moon configurations which form from impact-generated disks are typically unstable: these systems will likely evolve into a single moon state as the moons mutually collide or as the inner moonlet crashes into the Earth.

Subject headings: planets and satellites: general — planets and satellites: individual — solar system: formation — Moon

1. INTRODUCTION

The "Giant-Impact" scenario proposes that the impact of a Mars-sized body with early Earth ejects enough material into Earth orbit to form the Moon (Hartmann and Davis 1975, Cameron and Ward 1976). Of all lunar origin theories, the giant-impact theory seems best able to account for the geochemical, geophysical and dynamical characteristics of the Earth/Moon system. Published works have utilized smoothed-particle hydrodynamics to model the impact event and the creation of an impact-generated protolunar disk (*e.g.* Cameron and Benz 1991 and Cameron 1997). These works predict the formation of an extremely hot debris disk with a mean radius near or interior to the classical Roche limit for lunar density materials ($\sim 2.9\mathrm{R}_\oplus$) and an outer disk edge of $\sim 20R_\oplus$. To date, few works have addressed the earliest evolution of this disk, which may have experienced instability-enhanced viscous spreading prior to cooling and solidification (Ward and Cameron 1978 and Thompson and Stevenson 1989).

The mid-phase of disk evolution–when material has cooled and settled enough to allow for collisional growth–has been studied in Canup and Esposito (1996, hereafter CE96) and most recently in Ida *et al.* (1997, hereafter ICS97). The latter presented the first N-body simulations of accretion in a protolunar disk using a Hermite-scheme integrator to follow the orbital and collisional evolution of between 1000 and 2700 particles. ICS97 included tidal inhibition of accretional growth near the Roche limit by implementing the Canup and Esposito (1995) tidal accretion criteria, which basically require that a colliding pair of objects 1) not physically overflow their mutual Hill sphere and 2) rebound with a velocity less than a three-body escape velocity in order for accretion to occur. ICS97 varied initial disk masses and radial surface density profiles, as well as assumed values for the coefficient of restitution. Initial particle radii ranged from 38 to 380 kilometers, and most runs assumed a differential mass power-law index of $q_m = 1.5$ for the starting size distribution.

ICS97 found that the largest moonlet which accretes from the disk forms at a characteristic distance of between $1.2 - 1.5$ times the Roche radius (at the outer edge of the Roche zone) in about one year (or about 1000 orbits). This result was relatively independent of initial disk conditions and collisional parameterizations. Perturbations by the largest moonlet(s) were very effective at clearing-out inner disk material–in all of the ICS97 simulations, the smaller debris within the Roche zone was scattered either into the Earth or into a collisional orbit with the largest moonlet(s).

Two-thirds of the ICS97 runs end with a single large moonlet at $1.2 - 1.5a_{Roche}$ ($3.5 - 4.3R_{\oplus}$), together with multiple smaller bodies in exterior orbits. One-third of their simulations, typically those which began with the most radially-extended disks, yielded systems with two large moonlets (*i.e.*, with $m_2 \gtrsim 0.3m_1$). At the end of these cases, the more massive moonlet had an orbital radius of $a \sim .8$ to $2a_{Roche}$ ($2.32 - 5.8R_{\oplus}$). Figures 1 and 2 show example results from ICS97 for the one and two-moon cases. Resulting inclinations of the largest moonlet(s) were always low, while typical eccentricities were $\lesssim 0.1$ for the one-moon cases and higher for two-moon cases ($\sim 0.09 - 0.4$). The ICS97 integrations did not include orbital evolution due to tidal interaction with the Earth.

This paper seeks to address a likely final stage of evolution in an impact-generated protolunar-disk: the tidal evolution of and mutual interactions between multiple bodies which have formed via accretion. Would a multiple moon system persist as it orbitally evolves? The dependence of the rate of orbital evolution on moonlet mass suggests that if the innermost moon is the most massive it will likely overtake and sweep-up all exterior material (Cameron and Benz 1981, CE96). However, trapping of outer material in exterior mean-motion resonances could preclude mutual collisions even in this case. Furthermore, cases in both CE96 and ICS97 yield systems of multiple moons in which the innermost moonlet is often not the most massive (*e.g.* Figure 2).

In this work we utilize both analytic techniques and numerical integrations to characterize probable modes of evolution for a terrestrial multiple moonlet system. The combination of these complementary approaches is very helpful, as the theoretical analysis allows for straightforward categorizations of general outcomes for certain idealized cases (*e.g.* single, isolated resonances), while the numerical integrations reveal the complexities of the full N-body dynamics. The analytic methods and our numerical model are described in Sections II and III respectively. Our results are discussed in Section IV, and our conclusions are summarized in Section V.

2. ANALYTIC MODELING

Below we review the analytic modeling which we will utilize in conjunction with our numerical integrations to describe the evolution of a multiple moon terrestrial system. We benefit from the great amount of past work which has addressed the stability and evolution of the satellite systems of the outer planets (*e.g.* Greenberg 1977, Dermott *et al.* 1988, Tittemore and Wisdom 1988, 1989, 1990). A terrestrial multiple moon system differs dynamically from these systems in three key respects: a much larger mass ratio of satellites to central planet, a substantially faster rate of tidal evolution, and the significant effect of tides raised on the Earth on increasing satellite eccentricities. All of these factors help to explain our single Moon system. We note that here we assume satellites occupy co-planar orbits in the Earth's equatorial plane.

2.1. Tidal Evolution of Moonlets

2.1.1. *Terrestrial Tides*

For orbits outside synchronous orbit (typically $2.3R_\oplus$ immediately after the impact event), tides raised on the Earth by an orbiting satellite lead to a transfer of angular momentum from the Earth's rotation to the satellite's orbit, causing an increase in orbital radius. CE96 used a simple model of tidal evolution in order to predict when two moons would likely evolve into potentially collisional orbits, considering only the evolution of orbital radius due to the M_2 principal tides raised on the Earth:

$$\left.\frac{da}{dt}\right|_\oplus \approx 3k_2\sqrt{\frac{G}{\mathrm{M}_\oplus}}\mathrm{R}_\oplus^5 m a^{-11/2}\sin(2\delta) \tag{1}$$

where k_2 is the Earth's second order Love number, $\mathrm{M}_\oplus$ and $\mathrm{R}_\oplus$ are the mass and radius of the Earth, m and a are the mass and orbital radius of the orbiting body, and δ is the lag angle between the bulge raised on the Earth and point below the disturbing body (*e.g.* Burns 1986). Tides raised on the Earth also cause an evolution in eccentricity for initially non-circular orbits, with:

$$\left.\frac{de}{dt}\right|_\oplus \approx \mathrm{sgn}(\sigma)\frac{19\mathrm{e}}{8\mathrm{a}}\left.\frac{\mathrm{da}}{\mathrm{dt}}\right|_\oplus, \tag{2}$$

where $\sigma = (2\omega - 3n)$, ω is the angular rotation rate of the Earth, n is the satellite's mean motion, and σ is positive for $a \gtrsim 1.3a_{sync}$ (Kaula 1964; Goldreich and Soter 1966).

Integrating Eq. (1), CE96 determined when two bodies would tidally evolve into unstable orbits with $\delta a \leq 3.5R_{Hill}$ (*e.g.* Gladman 1993), where R_{Hill} is the mutual Hill radius of the interacting bodies ($R_{Hill} = a\left(\frac{m_1+m_2}{3\mathrm{M}_\oplus}\right)^{1/3}$). They found that the dynamical separation between two tidally evolving moonlets, $\delta a/a$, asymptotes to a value which is just a function of the mass ratio of the moonlets:

$$\left.\frac{\delta a}{a}\right|_{asym} = \left(\frac{m_2}{m_1}\right)^{2/13} - 1, \tag{3a}$$

where m_1 and m_2 are the masses of the inner and outer moonlets and $\delta a/a = (a_2 - a_1)/a_1$. The critical relation which determines whether two moonlets will converge or diverge to this asymptotic value is a function of just their masses and initial positions:

$$\left.\frac{m_1}{m_2}\right|_{crit} = \left(\frac{a_1}{a_2}\right)^{13/2}, \tag{3b}$$

where a_1 and a_2 are the moonlet orbital radii and $a_1 < a_2$. For (m_1/m_2) greater than this value, the moonlet orbits converge. For systems with $(m_1 + m_2) = .1 - 1M_{lunar}$, a mass ratio $(m_1/m_2) \gtrsim 0.06 - 0.22$ is required for the asymptotic separation value to be $\leq 3.5R_{Hill}$, or in order for two moonlets to evolve into potentially collisional orbits. While their analysis included only tidal effects on orbital radius and used a very symplistic stability criterion, the expressions in Eq. (3a-b) will be useful in our expanded treatment here.

2.1.2. Satellite Tides

In addition to the effects of terrestrial tides, an orbiting body will also be affected by tides raised by the Earth on the satellite. Tides raised on a synchronously rotating satellite (*i.e.* with $n = \omega_s$ where ω_s is the rotation rate of the satellite) in a circular orbit will form in line with the centers of the satellite and the Earth, and so will not yield any torque. However, for non-circular orbits the satellite tides dissipate energy as their magnitude varies from perigee to apogee and as the satellite bulge position is alternately ahead of and behind the line of centers. Both the radial "push-pull" tides and the "wobble" tides tend to circularize satellite orbits, competing with the effects of planetary tides for orbits outside co-rotation (*e.g.* Burns 1986).

From Kaula (1964) and Goldreich and Soter (1966), the rate of change of eccentricity due to both Earth and satellite tides (assuming all tidal components have the same lag angle) is:

$$\left.\frac{de}{dt}\right|_t \approx \frac{19e}{8a}\left.\frac{da}{dt}\right|_{\oplus}[\mathrm{sgn}(\sigma) - \frac{28}{19}\mathrm{A}], \tag{4}$$

where $\frac{da}{dt}|_{\oplus}$ is given in Eq. (1), $\sigma = (2\omega - 3n)$, and A is defined as

$$A = \frac{k_2^* \sin(2\delta^*)}{k_2 \sin(2\delta)} \left(\frac{M_{\oplus}}{m}\right)^2 \left(\frac{R^*}{R_{\oplus}}\right)^5, \tag{5}$$

the ratio of satellite-to-planet effects used in Mignard (1980, 1981; see also Kaula 1964 and Burns 1986), where the starred quantities are those of the satellite. For the current Earth-Moon system, $(k_2/Q)_{lunar} \approx 0.0011$, $(k_2/Q)_{\oplus} \approx 0.021$, and so $A \sim 0.5$ (Burns 1986, Dickey *et al.* 1994). A range of A values from 0 to 20 is used to represent the range of plausible values during the Moon's evolutionary history; the former corresponds to no satellite dissipation while the latter corresponds to the limit when only solid body tides in the Earth contribute to terrestrial dissipation ($Q_{\oplus} \sim 300$). The value of $Q_{\oplus}$ has certainly changed over the course of the Moon's history, as its current value implies that the Moon achieved its present position after only about 2 billion years (see Burns 1986).

2.2. Mean-Motion Resonances Between Moonlets

As moonlets orbitally evolve due to tides they will pass through mutual mean-motion resonances. In theory, passage through resonance could either increase or decrease the stability of a multiple satellite system relative to that predicted from only relative rates of tidal evolution. For instance, the satellite systems of the outer planets exhibit an unusually high number of long lived locked resonant configurations (*e.g.* Goldreich 1965). Passage through resonances is typically modeled by treating tidal effects as a slow, adiabatic evolution of semi-major axis which affects a single-resonance Hamiltonian (*e.g.* Henrard and Lemaitre (1983), Borderies and Goldreich (1984), Peale (1986) and Malhotra (1994)). The evolution of the system during passage through or capture into an isolated resonance can then be described by means of the adiabatic theorem. In this work we investigate the effects of mean-motion eccentricity resonances, but note that other classes of resonances (*e.g.* secular or inclination resonances) may also be important.

A mean-motion resonance occurs when the ratio of the mean motions of two bodies is nearly a ratio of integers, *e.g.* for the $(p+q):p$ resonance, $n_1/n_2 \approx (p+q)/p$ where n is mean motion and q is the order of the resonance. During a mean-motion eccentricity resonance, the gravitational interaction between the two bodies acts to maintain their conjunction at a certain longitude relative to the apse of one or both of the bodies. This process causes the critical argument of the resonance, ϕ, to librate about a fixed angle.

For every mean-motion commensurability there are several states which are each defined by their own critical argument, which for co-planar orbits is just: $\phi = -p\lambda_1 + (p+q)\lambda_2 - q_1\tilde{\omega}_1 - q_2\tilde{\omega}_2$, where λ_1 and λ_2 are the mean longitudes of the inner and outer body, $\tilde{\omega}_1$ and $\tilde{\omega}_2$ are the longitudes of pericenter of the inner and outer bodies, and q_1 and q_2 are integers with $(q_1+q_2)=q$ (see Malhotra 1994). For first and second order resonances between co-planar bodies, there are 3 primary resonance states for a given $(p+q):p$ commensurability to second order in eccentricity, and in general, the relative masses and eccentricities of the two bodies determine which state is occupied. For the 2:1 resonance, the "e_1" state is characterized by $\phi_{e_1} = -\lambda_1 + 2\lambda_2 - \tilde{\omega}_1$, the "$e_2$" state by $\phi_{e_2} = -\lambda_1 + 2\lambda_2 - \tilde{\omega}_2$, and the second-order 4:2-e_1e_2 state by $\phi_{e_1e_2} = -2\lambda_1 + 4\lambda_2 - \tilde{\omega}_1 - \tilde{\omega}_2$. For the $2:1$ commensurability and low eccentricities, the e_1 state is associated with $m_2 >> m_1$ (an interior resonance), while the e_2 state (exterior resonance) is associated with $m_1 >> m_2$.

Standard theories for evolution through resonance assume that the primary states of a given commensurability are "well separated", or that the variation of semi-major axis that results from the resonance interaction (the libration width) is small compared to the radial separation of neighboring resonance states (*e.g.* Dermott *et al.* 1988). The separation of the primary states of a commensurability occurs mainly due to differences in precession rates associated with the oblateness of the primary. The libration width of a given state depends both on the mass ratio of the secondary to the primary, and on e^q. When the secondary-to-primary mass ratio is small and J_2 is large, even low-order resonances are well-separated (Dermott *et al.* 1988). However, when J_2 is small this is not necessarily the case. In a group of three papers, Tittemore and Wisdom (1988, 1989, and 1990) demonstrated that single-resonance theory was inadequate to describe passage through and capture in resonances in the Uranian system, where J_2 is small. In particular, they identified significant chaotic zones surrounding low-order resonances, and found that escape from resonance could occur even after long periods of stability and in cases where single-resonance theory would predict permanent capture. In our analytic analysis here we have utilized the single-resonance theory, which is conservative in that it will tend to overestimate stability. Even given this approach, we find all likely initial moonlet configurations to be unstable.

2.3. Capture into Resonance

When two moonlets orbitally evolve through an isolated mean-motion resonance, the outcome is dependent upon whether their orbits are converging or diverging (*i.e.* whether $\frac{d}{dt}(\delta a/a)$ due to tides is negative or positive). Resonant perturbations tend to increase the orbital separation between the resonant bodies. If the orbits of two bodies are diverging as they tidally evolve, both resonant and tidal effects are additive and resonance trapping does not occur (*e.g.* Weidenschilling and Davis 1985). In this case, passage through the resonance results in a jump in eccentricity whose magnitude may be estimated from adiabatic analysis (see Dermott *et al.* 1988 or Peale 1986).

For tidally converging orbits, a resonant configuration can be maintained under certain conditions. First, the rate of tidal evolution must be slow enough so that the change in a due to tides in one libration period of the resonance is much less than the amplitude of the resonant perturbation of a–this is the "adiabatic criterion" (see Dermott *et al.* 1988, Malhotra 1993). For tidal evolution rates which greatly exceed this limit, passage through resonance without capture occurs. With $Q_\oplus \gtrsim 10$, the adiabatic condition is met for the first and second order resonances ($q = 1, 2$) considered here. If the adiabatic criterion is satisfied, capture into an isolated resonance is certain if eccentricity values far away from resonance are below a critical value. For initial eccentricites higher than this value, capture into resonance is probabilistic. The value of the critical eccentricity depends on the resonance, the masses of the two bodies, and their orbital radii; exact expressions for this e_{crit} for first and second order resonances are found in Dermott *et al.* (1988, Appendix B; also Peale 1986 and Borderies and Goldreich 1984). For example, e_{crit} for capture into a first order interior resonance is:

$$e_{crit} = \left(\frac{2\sqrt{6}(m_2/M_\oplus)\alpha f(\alpha)}{p^2 + (p+1)^2(m_1/m_2)\alpha^2}\right)^{1/3}, \qquad (6)$$

where $\alpha = a_1/a_2$ and $f(\alpha)$ is a function of Laplace coefficients (Brouwer and Clemence 1961, pp. 490-494; also see Weidenschilling and Davis (1985) for $q = 1$ values: their $C(\alpha) = 2f(\alpha)$). Capture probability decreases with increasing e for $e > e_{crit}$.

Thus we can 1) utilize the CE96 criterion for convergence/divergence to determine what mass ratio moonlets may get captured into a given resonance and 2) estimate critical eccentricities for capture into resonance for the convergent cases. Figure 3 is a plot of the asymptotic (a_1/a_2) value due to tidal evolution as a function of moonlet mass ratio; also shown are the locations of first and second order mean-motion resonances. Stable capture into resonance is impossible in the phase space above the solid curve, since here orbits are diverging to their asymptotic tidal separation. Below the solid curve orbits are tidally converging, and capture is certain if $e < e_{crit}$ and probabilistic otherwise. Also shown is the critical (a_1/a_2) ratio for two-body stability ($\delta a \leq 3.5 R_{Hill}$) for $(m_1 + m_2) = M_{lunar}$. *Because of the large mass ratio of the Moon to the Earth, the only first and second order commensurabilities which lie outside the two-body stability separation for bodies which total a lunar mass are the 2:1, 4:2 and the 3:1.*

2.4. Evolution in Resonance

The evolution of tidally evolving bodies once captured in resonance has been modeled by multiple past works (*e.g.* Peale 1986, Dermott *et al.* 1988, Pauwels 1994). We have specifically compared our numerical results to the analytical predictions from both Pauwels (1994) and Dermott *et al.* (1988). Here we follow the approach used in the latter work, as it easily allows for the inclusion of effects due to both terrestrial and satellite tides.

From Dermott *et al.* (1988), the averaged rates of change of eccentricity due to the resonant interaction between two tidally evolving bodies trapped in an isolated mean-motion resonance (with $\phi = -p\lambda_1 + (p+q)\lambda_2 - q_1\tilde{\omega}_1 - q_2\tilde{\omega}_2$), are:

$$\left\langle \frac{de_1}{dt} \right\rangle \bigg|_r = \frac{-\sqrt{1-e_1^2}}{e_1} n_1 a_1 \frac{m_2}{M_\oplus} \frac{F}{3g} \left[q_1 + p(1 - \sqrt{1-e_1^2}) \right] \tag{7}$$

$$\left\langle \frac{de_2}{dt} \right\rangle \bigg|_r = \frac{-\sqrt{1-e_2^2}}{e_2} n_2 a_2 \frac{m_1}{M_\oplus} \frac{F}{3g} \left[q_2 - (p+q)(1 - \sqrt{1-e_2^2}) \right]. \tag{8}$$

The function g is just

$$g = p^2 \frac{Gm_2}{a_1^2} + (p+q)^2 \frac{Gm_1}{a_2^2} \approx p^2 \frac{Gm_2}{a_1^2} \left[1 + \frac{a_2 m_1}{a_1 m_2} \right]. \tag{9}$$

The expression for F is

$$F = p\dot{n}_{1,t} - (p+q)\dot{n}_{2,t}, \tag{10}$$

where $\dot{n}_{1,t}$ and $\dot{n}_{2,t}$ are the rates of change of the mean motions of the inner and outer satellites due to tides. For tidally converging orbits (necessary for capture into resonance in the first place), F is negative and is dominated by the first term (*e.g.* for $a_1/a_2 \sim 0.5$ the first term is an order of magnitude larger than the second term for $m_1/m_2 \gtrsim 0.1$). The rate of change in n_1 due to tides is just

$$\dot{n}_{1,t} = -\frac{3n_1}{2}\left(\frac{\dot{a}_{1,t}}{a_1}\right), \tag{11}$$

where $\dot{a}_{1,t}$ is the rate of change of a_1 due to all tidal effects.

The $\dot{a}_{1,t}$ rate in Eq. (11) contains contributions due to both planetary and satellite tides. Assuming tides in the satellite dissipate energy while conserving angular momentum,

$$\left.\frac{da_1}{dt}\right|_s = \frac{2a_1e_1}{(1-e_1^2)}\left.\frac{de_1}{dt}\right|_s, \tag{12}$$

where $de_1/dt|_s$ is the rate of change of eccentricity of the inner satellite due to tides raised on the satellite, so that the total rate of change of a_1 due to both satellite and Earth tides is given by

$$\left.\frac{da_1}{dt}\right|_t = \left.\frac{da_1}{dt}\right|_\oplus\left[1 - \frac{7e_1^2A}{(1-e_1^2)}\right]. \tag{13}$$

The total rate of change of the eccentricity of a satellite in a mean-motion resonance is a combination of the effects due to the resonance (Eqs. (7)-(8)) and those due to tides raised on both the Earth and the satellite (Eq. (4)). These analytic evolution rates are compared to our numerical results described below. For sufficiently high values of satellite dissipation (*i.e.* high A values), an equilibrium eccentricity is reached. For $m_1/m_2 \gtrsim 0.1$ and $F \approx p\dot{n}_{1,t}$, the equilibrium eccentricities to lowest order in e can be solved for explicity and are given by:

$$e_{1,eq}^2 = \frac{q_1}{p}\left[(7A - \frac{19\mathrm{sgn}(\sigma)}{4})(1 + \frac{a_2m_1}{a_1m_2}) + 7A\frac{q_1}{p}\right]^{-1}, \tag{14}$$

where $\sigma = (2\omega - 3n)$, and

$$e_{2,eq}^2 = \frac{q_2}{p}\left(\frac{m_1}{m_2}\right)^2\left(\frac{a_2}{a_1}\right)^6\left(1 - 7e_{1,eq}^2A\right)\left[(7A - \frac{19\mathrm{sgn}(\sigma)}{4})(1 + \frac{a_2m_1}{a_1m_2})\right]^{-1}. \tag{15}$$

Eq. (14) is equivalent to Tittemore and Wisdom (1990) Eq. (53), except in that case they did not include the effect of planetary tides on satellite eccentricity, as this is unimportant for satellites orbiting gaseous planets with high Q values. For $m_1 \gg m_2$ (exterior resonance case), the first term in g can be neglected and the equilibrium eccentricity of the outer body can again be explicity solved for to lowest order in e:

$$e_{2,eq}^2 = \frac{q_2 p}{(p+q)^2}\left(\frac{m_1}{m_2}\right)\left(\frac{a_2}{a_1}\right)^8 (1 - 7e_1^2 A)\left[7A - \frac{19\mathrm{sgn}(\sigma)}{4}\right]^{-1}. \quad (16)$$

Note that the equilibrium eccentricities depend only on moonlet mass ratio, the type of resonance, and the A value.

Thus from analytic methods we can determine which mutual mean-motion resonances moonlets can become captured in (and with what capture probability for $e > e_{crit}$) as they orbitally evolve due to both planetary and satellite tides. Given that capture into an isolated resonance occurs, we can then estimate the subsequent evolution of moonlet eccentricities (due to both tides and the resonant interaction) from the rates given in Eqs. (4), (7) and (8). Despite the simplifying assumptions inherent to these methods, they provide a clarifying structure in which to categorize the numerical results.

3. NUMERICAL ANALYSIS

To simulate the evolution of multiple moonlet systems we utilize a code developed as part of the SWIFT group of integrators which uses the mixed variable symplectic (MVS) orbit integrator developed in Wisdom and Holman (1991) (see also Levison and Duncan 1994). This symplectic technique by its N-body nature implicitly accounts for the effects of mutual interactions, including resonances. For this work, the orbiting satellites are additionally accelerated by tides raised on the Earth at each time step (see Touma and Wisdom 1994). Accelerations due to tides raised on the orbiting satellites are not included in our numerical simulations, due to difficulties in incorporating the evolution of satellite rotation in our symplectic method. In particular, tracking of the moonlet spin rates is necessary for the proper treatment of the "wobble" component of the satellite tides, especially in the case of very eccentric orbits.

3.1. Tidal Accelerations

The tidal-generating force of a satellite in Earth orbit causes the Earth to assume a distorted shape relative to the sub and anti-satellite points, which can be mathematically described in terms of an increase in the second-order harmonic of the Earth's gravitational potential. As a result of dissipation within the Earth, the bulge achieves a maximum height some time Δt after the tide raising impulse from the satellite. For a satellite outside geosynchronous orbit, the tidal bulges will lead ahead of the line through the satellite-Earth centers by an angle δ which is a function of Δt: $\delta = (\omega - n)\Delta t$. While the tidal potential is often derived by assuming a constant lag angle, for our numerical integrations we follow the formalisms used by Mignard (1979, 1980, and 1981), Conway (1982), and Touma and Wisdom (1994) which instead assume a constant value for Δt, the characteristic time for bulge formation. This approach is preferred since the value of the lag angle δ is not constant for eccentric orbits and is of course a function of position relative to synchronous orbit.

The potential at a geocentric distance $\vec{r}$ due to the tidal distortion of the Earth raised by a satellite of mass m is just

$$U(\vec{r}) = \frac{Gk_2 m R_\oplus^5}{2r_p^5 r^5}[3(\vec{r}\cdot\vec{r_p})^2 - r^2 r_p^2] \tag{17}$$

where $\vec{r}_p$ was the position of the tide-raising body when the tide-raising impulse occurred at time $(t - \Delta t)$ (Conway 1982, Touma and Wisdom 1994). In order to determine the acceleration of the satellite by the bulge it has raised, one must determine the potential at the satellite's new position at the time the bulge forms, $\vec{r}_s$, where $\vec{r}_p = \vec{r}_s - \dot{\vec{r}}_s \Delta t$. Substituting this expression for $\vec{r}_p$ into Eq. (17), expanding to first order in Δt, and taking the gradient of $U(\vec{r})$ yields the acceleration:

$$\ddot{\vec{r}} = \frac{-3k_2 G m R_\oplus^5}{r^{10}} \Delta t [2\vec{r}(\vec{r} \cdot \vec{v}) + r^2(\vec{r} \times \vec{\omega} + \vec{v})], \tag{18}$$

where $\vec{r}$ is now the position of the satellite, and we have assumed that $\vec{r} = \vec{r}_s$, or that the object being accelerated is the same as the one which generated the tidal distortion (*e.g.* Conway 1982; Touma and Wisdom 1994). For multiple satellite systems, it is customarily assumed that each body is only affected by the tidal bulges it itself has raised on the central planet. This is because a satellite's own tidal bulges maintain a fixed position relative to the satellite, while bulges raised by other satellites would not and their changing relative orientations would tend to cause their effects to cancel out.[1]

We incorporate the tidal acceleration into our integrations at each time step ($\Delta \vec{v} = \ddot{\vec{r}}_{tides} t_{step}$) by adding it to the interaction part of the MVS Hamiltonian (see Wisdom and Holman 1991). The tidal time delay for the Earth (we typically use the current value of $\Delta t \sim 12$ minutes), and the initial rotation rate of the Earth (ω) are input parameters for each run. The oblateness of the Earth is determined as a function of ω, with $J_2 = 1.08 \times 10^{-3} \left(\frac{\omega}{7.3 \times 10^{-5} rad/sec}\right)^2$. By using Eq. (18) directly in our numerical simulations, we avoid the complications of an elliptic element-based approach in which tidal effects are determined on a tide-by-tide basis. Our integrations thus account for all

[1]We note that this may not be a valid assumption in the case of two satellites in a mean-motion resonance. In this case each satellite would experience a periodic interaction with the tidal bulge of the other satellite during their mutual conjunction, and this "tidal resonance" could result in an additional acceleration to both bodies (Craig Agnor, personal communication). We ignore such interactions here.

effects of a second-order $(l = 2)^2$ tidal distortion in the Earth's potential, as well as the J_2 harmonic due to rotational oblateness. Our $l = 2$ tidal acceleration expression is valid for any eccentricity or inclination.

As mentioned above, we do not include the effects of tides raised on the moonlets in our numerical integrations. Instead, the effects of satellite tides for various A values are estimated using the analytic methods described in Section II. We also ignore the effects of solar tides. Presently the torque on the Earth due to solar tides is one-fifth that of the lunar torque, and the relative importance of solar tides is even less for the much closer satellite orbits which we are concerned with here (Burns 1986, Mignard 1981).

4. RESULTS

We categorize our findings in terms of the relative moonlet masses, presenting both numerical and analytical results for each class. Unless otherwise stated, the numerical integrations assume a rotation rate of 5 hours, a terrestrial tidal time delay equal to its current value of $\Delta t \approx 11.54$ minutes, $A = 0$, and initially co-planar moonlet orbits. In most cases, the integrations were continued until the moonlets experienced a close encounter or one of the moons collided with the Earth. As before, our notation assumes $a_1 < a_2$.

---

[2]The $l = 3$ order terms decrease more rapidly with orbital radius than the $l = 2$ terms; even at the Roche radius for silicate densities ($a = 3R_\oplus$) the force due to the $l = 2$ distortion is a factor of ~ 5 greater than that due to the $l = 3$ terms (*e.g.* Mignard 1980).

4.1. Moonlets with $m_1 \gg m_2$

This configuration is predicted by about two-thirds of the ICS97 simulations, with a large single moonlet at the outer edge of the Roche zone and a small amount of mass contained in smaller, exterior debris. It has typically been assumed that a more massive inner moon will overtake and sweep up much smaller outer debris. However, stable capture of this debris into exterior resonances could prevent mutual collision.

Figure 4a shows the evolution of 2 moonlets with $(m_1/m_2) = 100$, $m_1 = 10^{25}$ g ($M_{lunar} = 7.349 \times 10^{25}$ g), a starting separation of about $7.6 R_{Hill}$ (just outside the 2:1 resonance) and initially circular orbits. Here and in subsequent figures, the black and green curves are orbital radii, while the yellow and orange curves indicate perigee and apogee at each time step, while positions of the (in order of increasing distance from the planet) 4:1, 3:1, 2:1 and 3:2 interior resonances are indicated by the brown curves (we note that only the latter three resonances are shown in Figure 4a due to the chosen ordinate scale). Times are shown in units of (seconds/808) and a is in Earth radii. In the simulation shown in Figure 4a, the outer moon is captured into the 2:1-e_2 resonance and experiences a secular increase in its eccentricity; after about 460 years ($t = 1.8 \times 10^7$) the moonlets are on crossing orbits. Since our numerical integrations assume $A = 0$, there is no process which damps eccentricity for ($2\omega > 3n$). If the resonance eventually destabilizes, or if e_2 was initially too large to allow for capture into the resonance ($e_{crit} \sim 0.096$ for the 2:1 in this case), the moonlet orbits will continue to converge due to tides and mutual collision is probable. For the case shown in Figure 4a, at $t = 4.8 \times 10^8$ (after about 12,300 years) the eccentricity of the outer moonlet has grown to about 0.6. At this point the resonance no longer protects the outer body from close encounters with the inner body (*e.g.* Morbidelli *et al.* 1995), and the moonlets experience a close encounter.

Figure 4b is the predicted evolution of e_2 from the analytic formalism for $A = 0$ (solid line) compared to the numerical results (plotted points). Would dissipation in the moonlets allow for a stable, equilibrium eccentricity in an external resonance? For the case shown in Fig. 4, Eq. (19) implies that e_2 would have an equilibrium value less than unity only for $A \geq 145$; Figure 4b shows the time evolution of e_2 for $A = 100$ (dashed line) predicted by our analytic rate expressions. More generally, equilibrium e_2 values in exterior eccentricity resonances are less than unity for $(m_1/m_2) > 20$ only for $A \gtrsim 20$, a nominal upper limit on A's value during the history of the Earth/Moon system.

Thus for reasonable values of the relative importance of satellite to terrestrial tides ($0 \leq A \leq 20$), external resonances with the protomoon would have been unstable for small exterior material. We predict eventual sweep-up of outer debris by an inner protomoon.

4.2. Tidally Converging Moonlets with $m_1 \lesssim m_2$

Figure 3 shows the critical mass ratio at a given orbital radius separation for tidally diverging/converging orbits. Here we consider cases with $(m_1/m_2) \lesssim 1$ such that the moonlets are initially on converging orbits due to tides (below and to the right of the curve in Fig. 3). The ICS97 two-moon cases (of which there were a total of 7 out of 21 simulations) fall into this category. Here we find that the end result is often dependent on the choice of the initial spin rate of the Earth, which determines the location of synchronous orbit, a_{sync}. All of the ICS97 two-moon cases have an inner moon whose perigee is $\lesssim 2.5 R_\oplus$. Synchronous orbit is at $\sim 2.3 R_\oplus$ for a nominal terrestrial day of 5 hours–this is a typical day length produced by impacts with close to the current angular momentum of the Earth/Moon system (*e.g.* Cameron and Benz 1991). For impacts with twice the angular momentum of the current Earth/Moon system (which may be favored due to their ability to place more material into Earth orbit, see CE96 and ICS97), a day length of 2.5 hours is more appropriate.

Figure 5a shows the evolution of the two-moon system shown in Figure 2 (ICS97, their Run 13); this was the ICS97 two-moon case with the largest value of a_1. Here $m_1 = 0.39 M_{lunar}$, $m_2 = 0.63 M_{lunar}$, $\delta a_{initial} \sim 7 R_{Hill}$, and we have assumed initially circular orbits. The moonlets are quickly captured into the 3:1-$e_1 e_2$ resonance. The inner moonlet is close enough to co-rotation that both planet and satellite tides are acting to decrease its eccentricity; however, there is still a net increase in e_1 due to the resonant interaction. From Figures 5a-b, at about $t = 1.51 \times 10^6$, perigee of m_1 falls briefly within co-rotation, and the inner moon at $t = 1.52 \times 10^6$ becomes trapped in the 4:1. Here again the resonance acts to increase e_1, until perigee of the inner moonlet falls within co-rotation,[3] at which point the orbit of m_1 circularizes and falls into the earth at $t = 1.58 \times 10^6$, or after about 40 years.

Figure 6 shows the characteristic outcome for integrations of two-moonlet cases when perigee of m_1 is initially inside co-rotation (the case shown is ICS97's Run 12). The inner moon immediately begins its decent, with a final collision with the Earth after only about 5 years.

If we consider a terrestrial day of 2.5 hours, $a_{sync} \sim 1.5 R_\oplus$. Figure 7 shows the evolution of the two moons from Figure 5 with $T_\oplus = 2.5$ hours. The moons are again captured into the 3:1-$e_1 e_2$ resonance, and experience a close encounter after about 3 years. We obtained a similar outcome for all our integrations of the ICS97 two-moonlet cases with $T_\oplus = 2.5$ hours.

Thus with $A = 0$, the inner moonlets predicted by ICS97 collide with the Earth for rotation rates corresponding to a system angular momentum close to the current value,

---

[3]For eccentric orbits the tidal interaction can be well approximated by an impulse at perigee, since the tidal force is $\propto r^{-7}$. This means that it is the relative location of perigee (not mean orbital radius) to co-rotation that determines the overall direction of the evolution.

while the moonlets mutually collide if the spin rate of the Earth is significantly faster than this. How would dissipation in the satellites affect these outcomes? The fate depicted in Figure 6 would change little. However, the resonant interactions in Figures 5 and 7 would be affected. Figure 8 shows the analytic predictions for $e_1(t)$ from the run shown in Figure 5 for $A = 0$, 1.0 and 10.0. For $A = 1.0$ and 10.0, perigee of m_1 remains outside of co-rotation. Once the moonlets have outwardly evolved so that de/dt due to terrestrial tides is positive ($a \gtrsim 1.3 a_{sync}$), equilibrium eccentricities predicted from Eqs. (14) and (15) for $A = 10.0$ are $e_{1,eq} \sim 0.05$, $e_{2,eq} \sim 0.29$; for $A = 1.0$, $e_{1,eq} \sim 0.24$ and $e_{2,eq}$ has a value greater than unity. Similar results apply for the $T_{\oplus} = 2.5$ hours run shown in Figure 7. For satellite dissipation rates corresponding to $A \lesssim 0.5 - 1$, the predicted equilibrium eccentricity of the outer moonlet in a 3:1 or 4:2-$e_1 e_2$ eccentricity resonance is greater than unity for moonlet mass ratios greater than $m_1/m_2 \gtrsim 0.3$. In the case of significant satellite dissipation (*i.e.* A values larger than the current value), a resonant configuration between two moons close in size may have persisted for a considerable length of time. However, such a configuration would likely have destabilized when A approached its current value. We predict that all of the specific multiple moonlet cases found in ICS97 would evolve into single moon systems for expected values of A and a_{sync}.

4.3. Tidally Diverging Moonlets with $m_1 < m_2$

Here we consider cases to the upper left of the curve in Figure 3; to first order, these would seem to be the cases most likely to yield a long-lived multiple moon system. Assuming the moons begin with a stable separation in orbital radius, further tidal evolution will generally increase their relative separations. Divergence due to tides precludes stable capture into resonances. The expected outcome is that the outer moon leaves the inner one behind, and that as long as the inner body is massive enough to keep outside of co-rotation (whose position would be determined by the dominant interaction with the more massive outer moon) we might expect the pair to survive indefinitely.

These expectations are most clearly met when $m_1 \ll m_2$, as shown in Figure 9 where $(m_1/m_2) = 0.01$ and $m_2 = 5 \times 10^{24}$ g. The jump in eccentricity as the inner body diverges across the 2:1 is very distinct, with a resulting $e_1 \sim 0.12$. For diverging orbits with initially low eccentricities, adiabatic analysis predicts a jump in eccentricity $\sim e_{crit}$, where here $e_{crit} \sim 0.1$ (see Dermott *et al.* 1988). For $(m_1/m_2) = 0.1$, we find a large variation in our numerical results from this symplistic scenario. In Figure 10, $(m_1/m_2) = 0.1$, $m_2 = 0.05M_{lunar}$, and the initial orbital separation is about $5R_{Hill}$. The moons diverge through the 3:2, experience corresponding increases in eccentricity, and after a brief excitation by the 4:7, they resume a potentially stable configuration. Figure 11a follows the same initial conditions (same m_1/m_2, a_1/a_2), only here the moons are initially farther away from the planet. The jump in free eccentricity as the moons diverge through the 3:2 is again very clear (post-passage $e_1 \sim 0.1$ from adiabatic theory). However in this run, later interaction with the 4:7 (t=1.3e9) perturbed the orbital radius of the inner moon to such an extent that it crossed the 2:1 (see Figure 11b). At the 2:1, the moonlet orbits are converging due to tides and capture into the 2:1-e_1 resonance occurs, followed by a secular increase in e_1 until the integration was stopped when the orbits crossed. The critical eccentricity for the 2:1 for these parameters is $e_{crit} \sim 0.09$, which yields a capture probability of about 10% for an initial eccentricity of ~ 0.19. Another run with identical moonlet masses and positions but with an initial outer moonlet eccentricity of $e_{2,0} = 0.1$ did not result in capture into the 2:1 in this way, and again left the moonlets on potentially stable orbits.

Figure 12 shows a run with $(m_1/m_2) = 0.1$, $m_2 = 0.07M_{lunar}$, an initial spacing of 4.2 Hill radii (just outside the 3:2). In this case, eccentricity increases associated with mutual perturbations bring perigee of the inner moon inside a_{sync} after about 2000 years (9×10^7 in our units), and the inner moon collides with the Earth. We note that the run shown in Figure 10 probably narrowly missed a similar fate, as perigee of the inner moon extended inward as far as about $2.6R_\oplus$.

We completed a total of nine integrations which followed moonlets on diverging orbits which would have all been predicted to be stable by the CE96 criterion. All but one of the $(m_1/m_2) = 0.1$ cases in this category were nevertheless unstable and ended with mutual collision or with one body colliding with the Earth. Stability of a two-moon system increases for $m_1 \ll m_2$, and this would be the most problematic configuration for resolution with our current one Moon system. However, recent accretion simulations (ICS97) indicate that this configuration is unlikely to have occurred: by the nature of the morphology of impact-generated disks, the protomoon or moons form in close orbits (at outer edge of Roche zone) and are very effective at scattering small inner debris onto the Earth (Figs. 1 and 2).

5. CONCLUSIONS

The purpose of this work has been to conduct a preliminary study of the stability of a terrestrial multiple moon system, using both analytical techniques and numerical integrations. In particular, we are interested in the stability of multiple moonlet configurations predicted by modeling of lunar accretion from an impact-generated disk. Our results indicate that all of the systems produced in ICS97 will likely yield a single moon for reasonable values of tidal parameterizations. Our general findings can be best categorized in terms of relative moonlet masses:

1) Massive inner moon/Small exterior debris In this scenario, orbits are converging due to tides and capture into mean-motion resonances can occur for low enough eccentricities. However, we find that exterior eccentricity resonances are unstable over the whole range of plausible relative rates of satellite and terrestrial tidal dissipation ($A \leq 20$). The assumption that a large inner moon will eventually overtake smaller exterior material as it tidally evolves outward is a good one. Thus we expect sweep-up of outer disk debris which persists at the end of the ICS97 simulations.

2) Two-moons with $m_1 \sim m_2$ Here capture into resonances can again occur for low enough initial eccentricites, and equilibrium values of moonlet eccentricites in resonance are achieved for high rates of satellite dissipation ($A \gtrsim 5 - 10$). However, in this case resonances destabilize as the relative importance of satellite to planetary tides approaches its current value ($A \lesssim 0.5 - 1$).

This configuration is predicted by one-third of the ICS97 simulations. In all of our integrations of the two-moon ICS97 cases, we find that the inner moon rapidly crashes into Earth ($\sim$ years) due to its proximity to synchronous orbit for a terrestrial day of 5 hours. For a more rapidly spinning Earth (as would be appropriate for an initial giant impact event with $\gtrsim 2 J_{E-M}$), the two-moon configuration could have persisted for some time and the eventual outcome may have been either a moonlet-moonlet collision or a moonlet-Earth collision. We note that the former outcome was assumed in the accretion efficiency estimates in ICS97 (their Fig. 5).

3) Inner small material/Massive exterior body In this case, orbits diverge due to tides and capture into resonance is precluded. This configuration is the one most likely to yield a stable, multiple moon system around the Earth. However this initial condition might never be achieved from accretion in an impact-generated, lunar-mass disk, since perturbations by the largest moon or moons which form are very effective at scattering inner debris onto the Earth (ICS97).

This study has highlighted the importance of several factors which predispose a terrestrial system to a single moon state. First is the rapid rate of orbital evolution of satellites due to tidal interaction with the Earth. Even for solid body $Q_\oplus$ values ($Q \sim$ 100's), a protomoon which forms close to the Earth evolves out to $a \sim 20R_\oplus$ (a typical outer limit for an impact-generated debris cloud; Cameron and Benz 1991) in only $10^7 - 10^8$ years. In contrast, tidal evolution rates around gas planets are $10^3 - 10^4$ times slower. Second, terrestrial Q values are within an order-of-magnitude of likely Q values for orbiting satellites. This means that the plausible range of "A values"–the relative role of satellite to planetary tides in effecting satellite eccentricity evolution–extends only up to $A \lesssim 20$, with a current value $A \sim 1$. For a satellite orbiting a gaseous planet, $A \sim 1000$. In a terrestrial system, planetary tides thus play an important role in increasing satellite eccentricities, which acts to destabilize resonances and to increase mutual collisions. Finally, the large mass-ratio of the Moon to the Earth, coupled with lunar formation from a central, impact-generated disk, appears to insure that small inner disk material inside the Roche radius is effectively scattered onto the Earth (ICS97). In the context of these basic characteristics, it is not difficult to imagine why systems of multiple moons and rings persist around the gas giants while at Earth we find our single Moon.

5.0.1. Discussion

Our investigations have been directed towards the general identification of stable vs. unstable configurations of terrestrial multiple moon systems, and not towards the prediction of specific end outcomes. Multiple additional processes need to be characterized in order to make our results more case-specific. The symplectic integration technique utilized here breaks down upon close approach between two bodies, and so our simulations are unable to track the evolution of systems until a physical collision actually occurs. A new symplectic technique recently developed (Duncan *et al.* 1998) promises to remedy this deficiency.

A self-consistent incorporation of tides raised on orbiting satellites into a numerical scheme would allow for a much more thorough examination of the effects of high early rates of satellite dissipation on system stability. This would be particularly important for the case of multiple moonlets which are close in size. Such an improvement would be warranted if results from higher resolution simulations of the impact event and improved disk accretion models continue to suggest high likelihoods of multiple moon configurations such as the "two-moon" cases found in ICS97. The variation in satellite tidal dissipation rates can also have a significant effect on outcomes of specific cases. For significantly high eccentricities and A values, da/dt due to tides is negative (see Touma and Wisdom 1998, their Figure 6). This would of course alter the analysis of when a given pair of moons is tidally diverging or converging. Such reversals in orbital evolution direction would likely be short-lived (see Touma and Wisdom 1998, their Figure 9), as high A values will act to decrease eccentricities.

We have investigated only the planar eccentric problem in this work, and our future work will explore the effects of moonlet inclinations on system evolution. We have also neglected the effects of Sun, which have recently been shown to have a significant influence even in the inner disk through the resonance between the lunar periapse precession rate and the Earth's orbital period around the sun (the "evection" resonance), which occurs at $a = 4.6R_{\oplus}$ (Touma and Wisdom 1998). Capture into this resonance is capable of producing large eccentricities for a lunar-sized body ($e \sim 0.1 - 0.5$ for $A = 0$ to $A = 10$) on a time scale of thousands of years.

Finally, our results are dependent on the specifics of the giant impact event itself.

Currently two impact scenarios have been shown to be capable of yielding sufficiently massive debris disks: impacts with an angular momentum $\gtrsim$2 times that of the current system, and impacts with an Earth which has not yet fully accreted (Cameron 1997b, Cameron and Canup 1998). Recent SPH simulations of these types of impacts often yield massive, gravitationally bound clumps of debris in stable orbits subsequent to the impact event (Cameron 1997, Cameron 1997b, and Cameron and Canup 1998). The existence of such clumps in the initial disk could cause the distribution of moonlets which accretes from the disk to vary from the ICS97 predictions. Additional accretion simulations are required to determine the typical number and sizes of moons which form in these recently modeled impact scenarios.

We wish to thank Jack Wisdom for a preprint, Shigeru Ida for his help with data from ICS97, Al Cameron for many fruitful discussions, and Matt Holman for a helpful review. R.M.C. was supported by NASA's Origins of Solar Systems program; H.F.L. and G.R.S. were supported by NASA's Planetary Geology and Geophysics program.

REFERENCES

Borderies, N. and P. Goldreich 1984. A Simple Derivation of Capture Probabilities for the J+1:J and J+2:J Orbit-Orbit Resonance Problems. *Celes. Mech.* **32**, 127-136.

Brouwer, D. and G.M. Clemence. *Methods of Celestial Mechanics*. Academic Press, New York 1961.

Burns, J. A. 1986. The Evolution of Satellite Orbits. In *Satellites*, (J. A. Burns and M. S. Matthews, Eds.), pp. 117-158. Univ. of Arizona Press, Tucson.

Cameron, A. G. W. 1997a. The Origin of the Moon and the Single Impact Hypothesis V. *Icarus* **126**, 126-137.

Cameron, A. G. W. 1997b. Extended Parameter Study of the Giant Impact. In *Lunar and Plan. Sci. XXVIII.*

Cameron, A. G. W. and W. Benz 1991. The Origin of the Moon and the Single Impact Hypothesis IV. *Icarus* **92**, 204-216.

Cameron, A. G. W. and R. M. Canup 1998. The Giant Impact Occurred during Earth Accretion. In *Lunar and Planetary Science XXIX.*

Cameron, A. G. W. and W. R. Ward 1976. The Origin of the Moon. In *Lunar and Planetary Science VII*, 120-122.

Canup, R. M. and L. W. Esposito 1995. Accretion in the Roche Zone: Co-Existence of Rings and Ringmoons. *Icarus* **113**, 331-352.

Canup, R. M. and L. W. Esposito 1996. Accretion of the Moon from an Impact-Generated Disk. *Icarus* **119**, 427-446.

Conway, B. A. 1982. On the History of the Lunar Orbit. *Icarus* **51**, 610-622.

Dermott, S. F., R. Malhotra, and C. D. Murray 1988. Dynamics of the Uranian and Saturnian Satellite Systems: A Chaotic Route to Melting Miranda? *Icarus* **76**, 295-334.

Dickey, J. O. *et al.* 1994. Lunar Laser Ranging: A Continuing Legacy of the Apollo Program. *Science* **265**, 482-490.

Duncan, M. J., H. F. Levison, and M. H. Lee. 1998. A Multiple Timestep Symplectic Algorthim for Integrating Close Encounters. *Astron. J.*, in press.

Gladman, B. 1993. Dynamics of Systems of Two Close Planets. *Icarus* **106**, 247-263.

Goldreich, P. 1965. An Explanation of the Frequent Occurrence of Commensurable Mean Motions in the Solar System. *Mon. Not. Roy. Astron. Soc.* **130**, 159-181.

Goldreich, P. and S. Soter 1966. Q in the Solar System. *Icarus* **5**, 375–389.

Greenberg, R. 1977. Orbit-orbit Resonances in the Solar System: Varieties and Similarities. *Vistas in Astr.* **21**, 209-239.

Hartmann, W. K. and D. R. Davis 1975. Satellite-sized Planetesimals and Lunar Origin. *Icarus* **24**, 504-515.

Henrard, J. and A. Lemaitre 1983. A Second Fundamental Model for Resonance. *Cel. Mech.* **30**, 197-218.

Ida, S., R. M. Canup and G. R. Stewart 1997. Lunar Accretion from an Impact-Generated Disk. *Nature* **389**, 353-357.

Kaula, W. M. 1964. Tidal Dissipation by Solid Friction and the Resulting Orbital Evolution. *Rev. Geophys.* **2**, 661-685.

Levison, H. F. and M. J. Duncan 1994. The Long-Term Dynamical Behavior of Short-Period Comets. *Icarus* **108**, 18-36.

Malhotra, R. 1993. Orbital Resonances in the Solar Nebula: Planetesimal Velocities. *Icarus* **106**, 264-273.

Malhotra, R. 1994. Nonlinear Resonances in the Solar System. *Physica D* **77**, 289-304.

Mignard, F. 1979. The Evolution of the Lunar Orbit Revisited, I. *Moon and Planets* **20**, 301-315.

Mignard, F. 1980. The Evolution of the Lunar Orbit Revisited, II. *Moon and Planets* **23**, 185-201.

Mignard, F. 1981. The Lunar Orbit Revisited, III. *Moon and Planets* **24**, 189-207.

Morbidelli, A., F. Thomas. and M. Moons 1995. The Resonant Structure of the Kuiper Belt and the Dynamics of the First Five Trans-Neptunian Objects. *Icarus* **118**, 322-240.

Peale, S. J. 1986. Orbital Resonances, Unusual configurations and Exotic Rotation States among Planetary Satellites. In *Satellites*, (J. A. Burns and M. S. Matthews, Eds.), pp. 159-223. Univ. of Arizona Press, Tucson.

Pauwels, Th. 1994. Final Tidal Evolution of Orbit-Orbit Resonances. *Cel. Mech.* **59**, 101-127.

Stevenson D. J. 1987. Origin of the Moon. *Ann. Rev. Earth Plant. Sci.* **15**, 271-315.

Thompson, C. and D. J. Stevenson 1988. Gravitational Instability in Two-Phase Disks and the Origin of the Moon. *Astrophys. J.* **333**, 452-481.

Tittemore, W. C. And J. Wisdom 1988. Tidal Evolution of the Uranian Satellites I. Passage of Ariel and Umbriel through the 5:3 Mean-Motion Commensurability. *Icarus* **74**, 172-230.

Tittemore, W. C. And J. Wisdom 1989. Tidal Evolution of the Uranian Satellites II. An Explanation of the Anomalously High Orbital Inclination of Miranda. *Icarus* **78**, 63-89.

Tittemore, W. C. And J. Wisdom 1990. Tidal Evolution of the Uranian Satellites III. Evolution through the Miranda-Umbriel 3:1, Miranda-Ariel 5:3, and Ariel-Umbriel 2:1 Mean-Motion Commensurabilities. *Icarus* **85**, 394-443.

Touma, J. and J. Wisdom 1994. Evolution of the Earth-Moon System. *Astron. J.* **108**, 1943-1961.

Touma, J. and J. Wisdom 1998. Resonances in the Early Evolution of the Earth-Moon System. *Astron. J.* **115**, 1653-1663.

Ward. W. R. and A. G. W. Cameron 1978. Disk Evolution within the Roche Limit. In *Lunar and Plan. Sci. IX*, 1205-1207.

Weidenschilling, S. J. and D. R. Davis 1985. Orbital Resonances in the Solar Nebula: Implications for Planetary Accretion. *Icarus* **62**, 16-29.

Wisdom, J. and M. Holman 1991. Symplectic Maps for the N-Body Problem. *Astron. J.* **102**, 1528.

This manuscript was prepared with the AAS LaTeX macros v4.0.

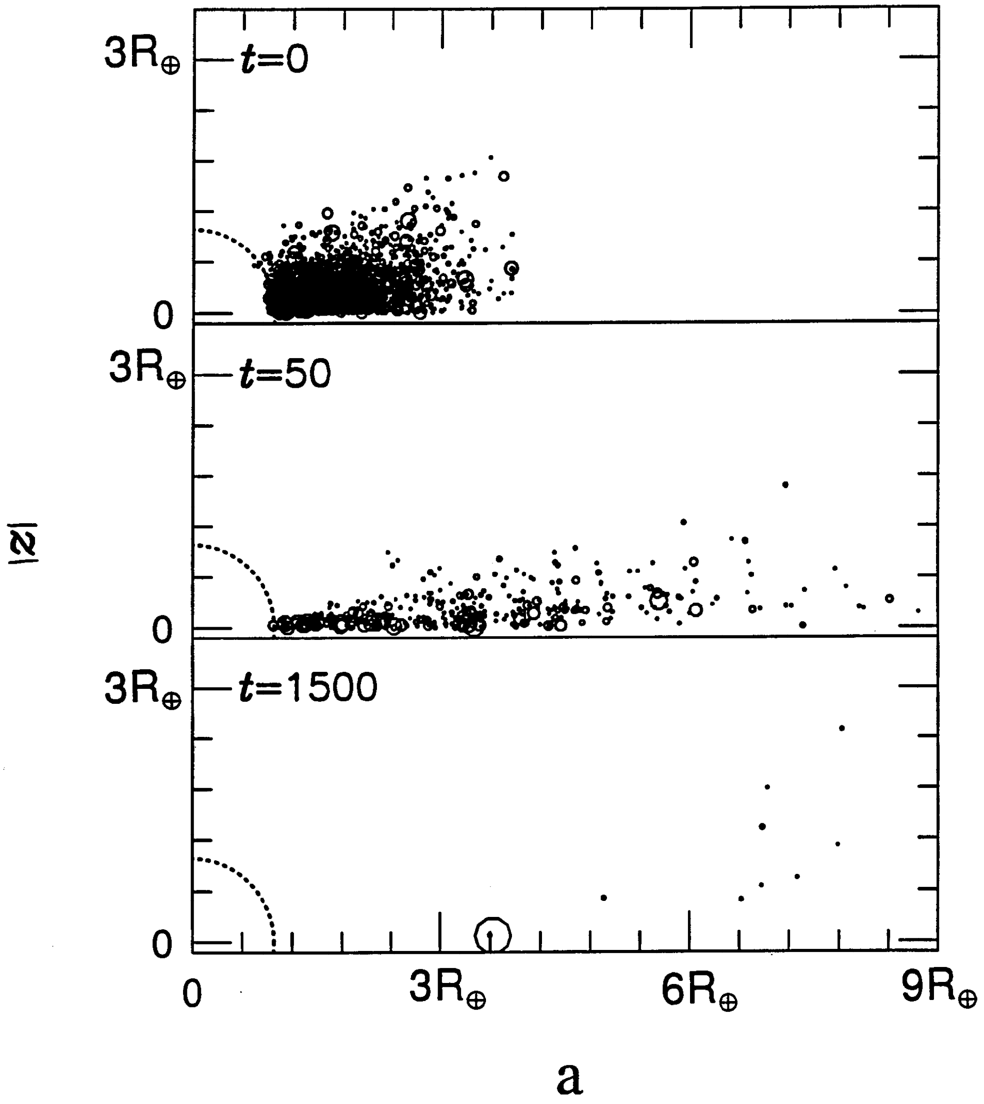

Fig. 1.— An example of the collisional evolution of an initially centrally-condensed protolunar debris disk (from ICS97, their Run 4). Cross-sections of the disk are shown at times t =0, 50 and 1500 orbits at $3R_\oplus$ (where 1500 orbits $\sim$ 15 months). The y-axis is the absolute value of the vertical height above the Earth's equatorial plane. The dashed semi-circle is the surface of Earth. The relative sizes of the disk particles are indicated, but are not shown to scale. The initial disk mass was 2.44 lunar masses; the largest moonlet which forms at $3.5R_\oplus$ has a mass of $0.4M_{lunar}$.

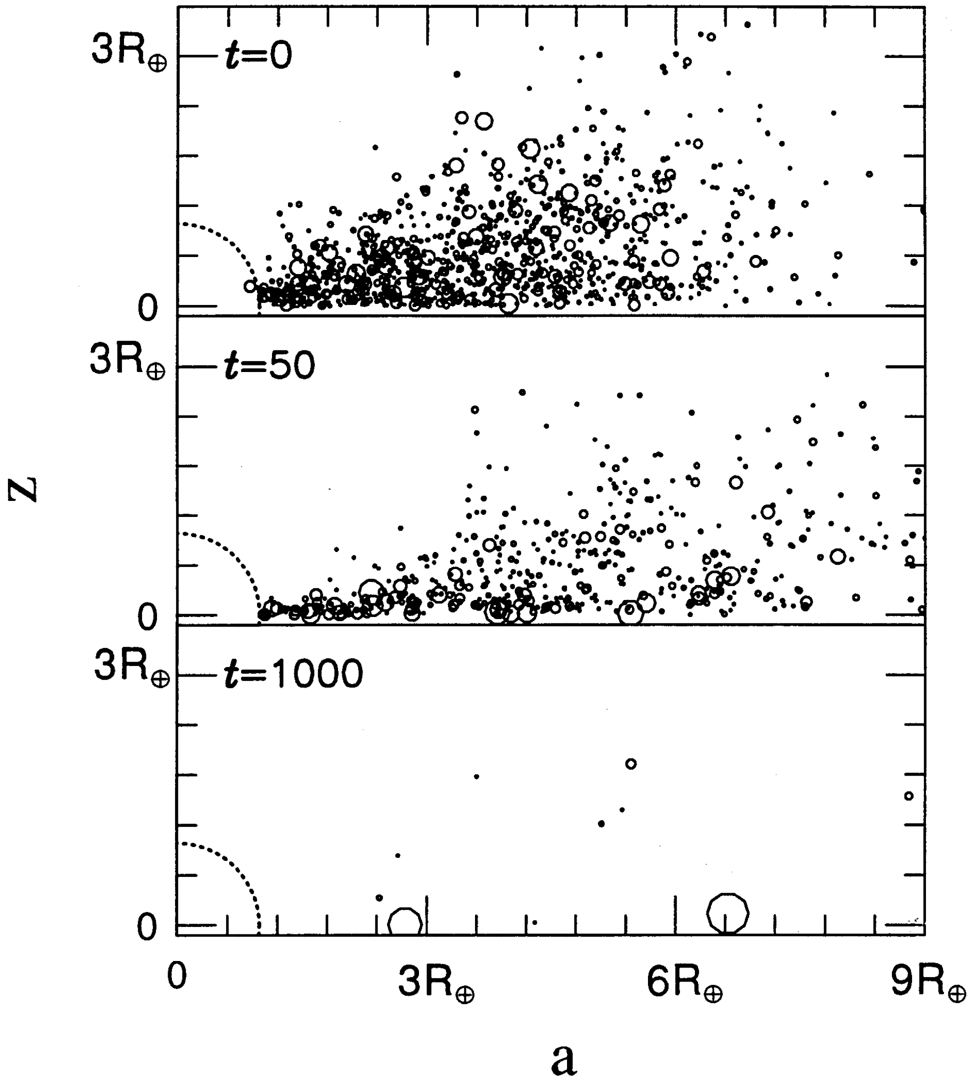

Fig. 2.— An example of the collisional evolution of a more radially extended protolunar debris disk (from ICS97, their Run 13). Cross-sections of the disk are shown at times t =0, 50 and 1000 orbits. The initial disk mass was again 2.44 lunar masses; the largest moonlet at $5.7R_{\oplus}$ has a mass of $0.63M_{lunar}$, while the inner moonlet at $2.7R_{\oplus}$ has a mass of $0.39M_{lunar}$.

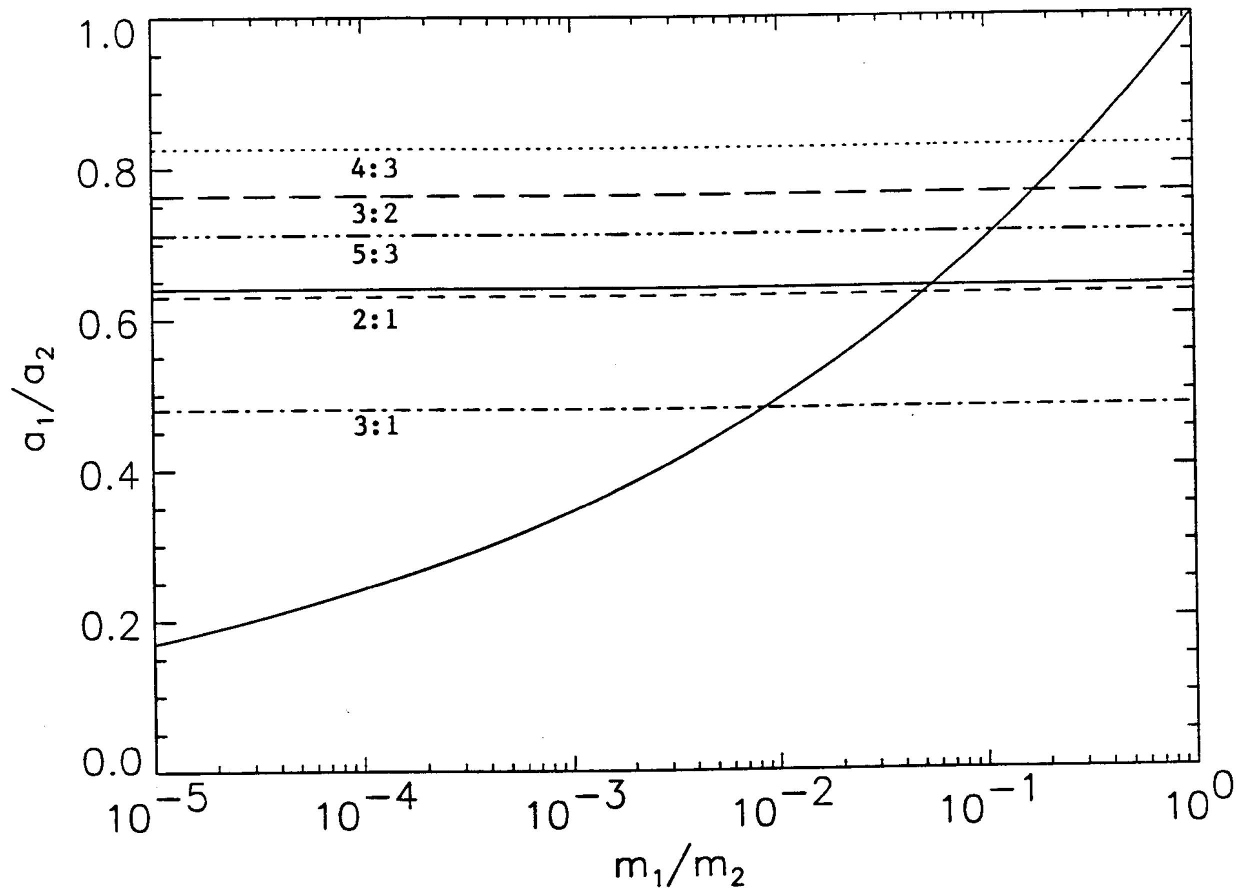

Fig. 3.— The solid curve is the asymptotic value of a_1/a_2 due to the principal terrestrial tide as a function of moonlet mass ratio. Above and to the left of the curve moonlet orbits diverge as they tidally evolve; below and to the right orbits converge due to tides. Also shown are the positions of first and second order mean-motion resonances. The solid horizontal line is the a_1/a_2 separation required for two-body stability with $(m_1 + m_2) = M_{lunar}$. The only first or second order resonances outside the $3.5R_{hill}$ stability separation in this case are the 3:1 and 2:1.

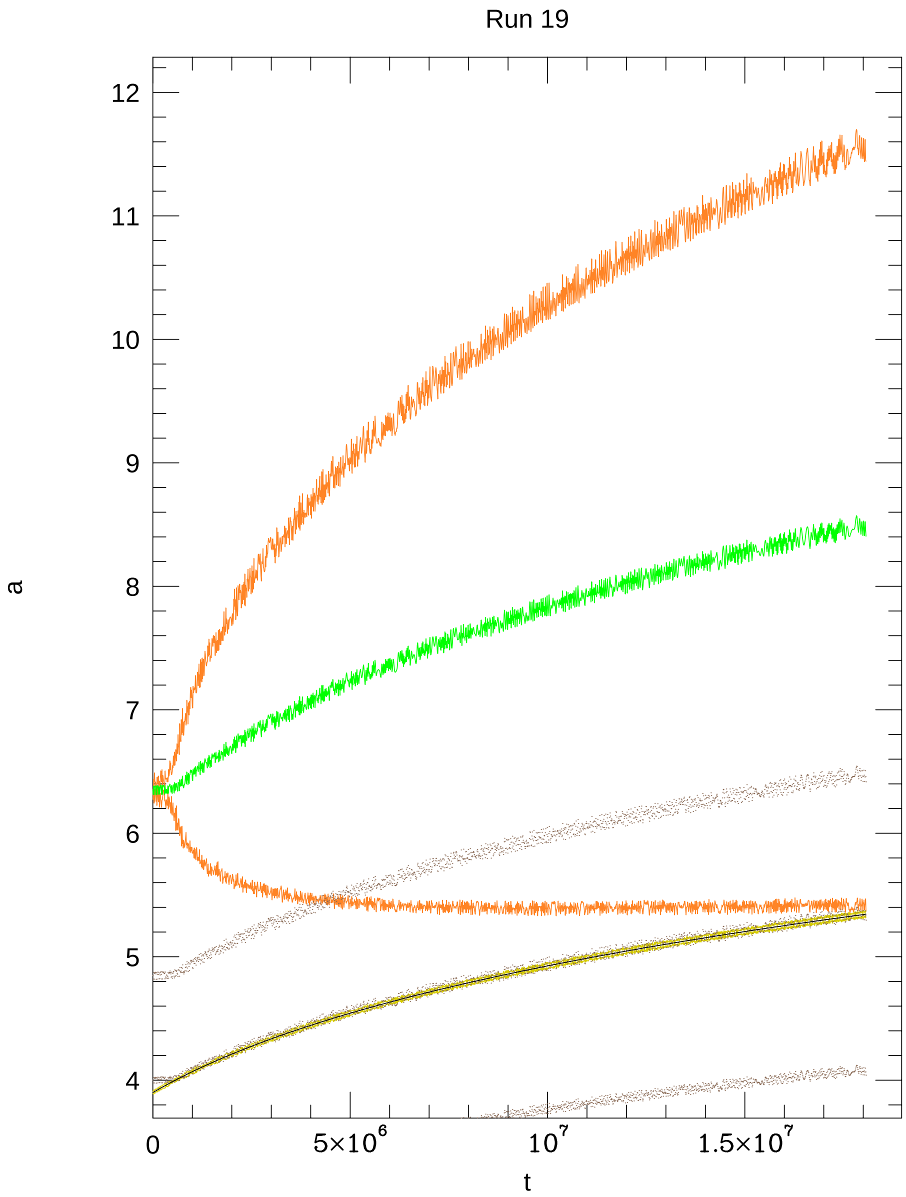

Fig. 4.— (a) Numerical simulation of the evolution of two moonlets ($m_1, m_2 = 10^{25}, 10^{23}$ g). The black and green curves are a_1 and a_2 respectively, while the yellow and orange curves show periapse and apoapse at each time step. The brown curves indicate the location of the 3:2 (at $\sim 4.8R_\oplus$ at $t = 0$), 2:1 (at $\sim 3.9R_\oplus$ at $t = 0$) and 3:1 interior mean-motion resonances. The y-axis is in Earth radii; the x-axis is (t(sec)/808). A terrestrial tidal time delay of $\Delta t = 11.54$ minutes and a terrestrial day of 5 hours were used. Effects of satellite tides are not included ($A = 0$). The moons are quickly captured into the 2:1-e_2 resonance, and e_2 continues to increase until the moons collide (at $t = 4.8 \times 10^8$). (b) **(NEXT PAGE)** Analytical predicted evolution of e_2 due to the 2:1-e_2 resonance for the case shown in (a) with $A = 0$ (solid line) and $A = 100$ (dashed line). Numerical results for $A = 0$ case are shown for comparison.

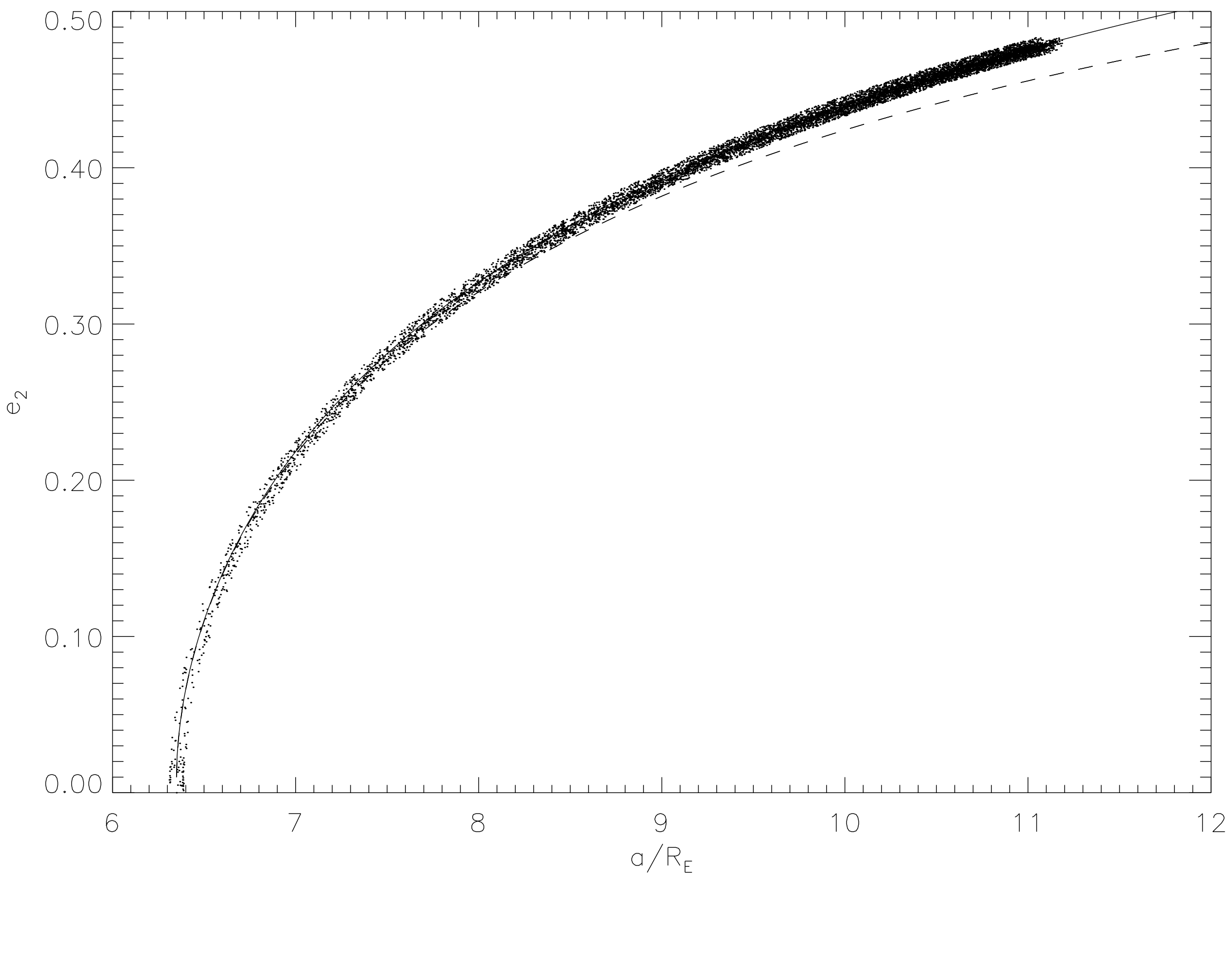
0.50
0.40
0.30
0.20
0.10
0.00
e_2
6
7
8
9
10
11
12
a/R_E

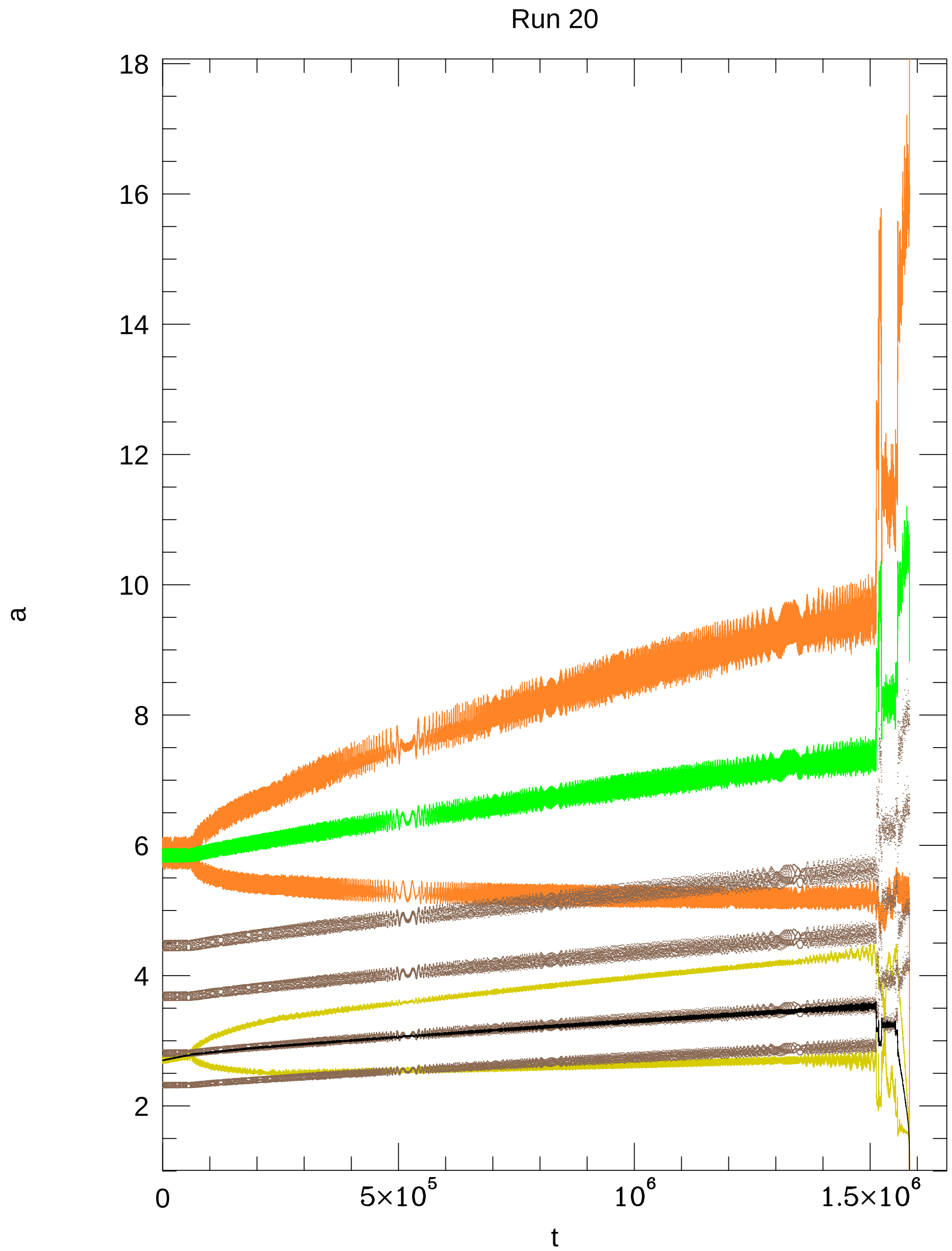

Fig. 5.— (a) Numerical integration of the evolution of the two-moonlet case from ICS97 shown in Figure 2 (their Run 13). A terrestrial day of 5 hours, or $a_{sync} = 2.33R_\oplus$ was assumed. Here the two moons are captured into the 3:1-e_1e_2 resonance until about $t = 1.5 \times 10^6$ (about 40 years). After a brief period of capture in the 4:1, perigee of the inner moon falls within synchronous orbit and its orbit then circularizes and falls into the Earth. (b) **NEXT PAGE** The evolution of relevant quantities from the simulation shown in Figure 5a.

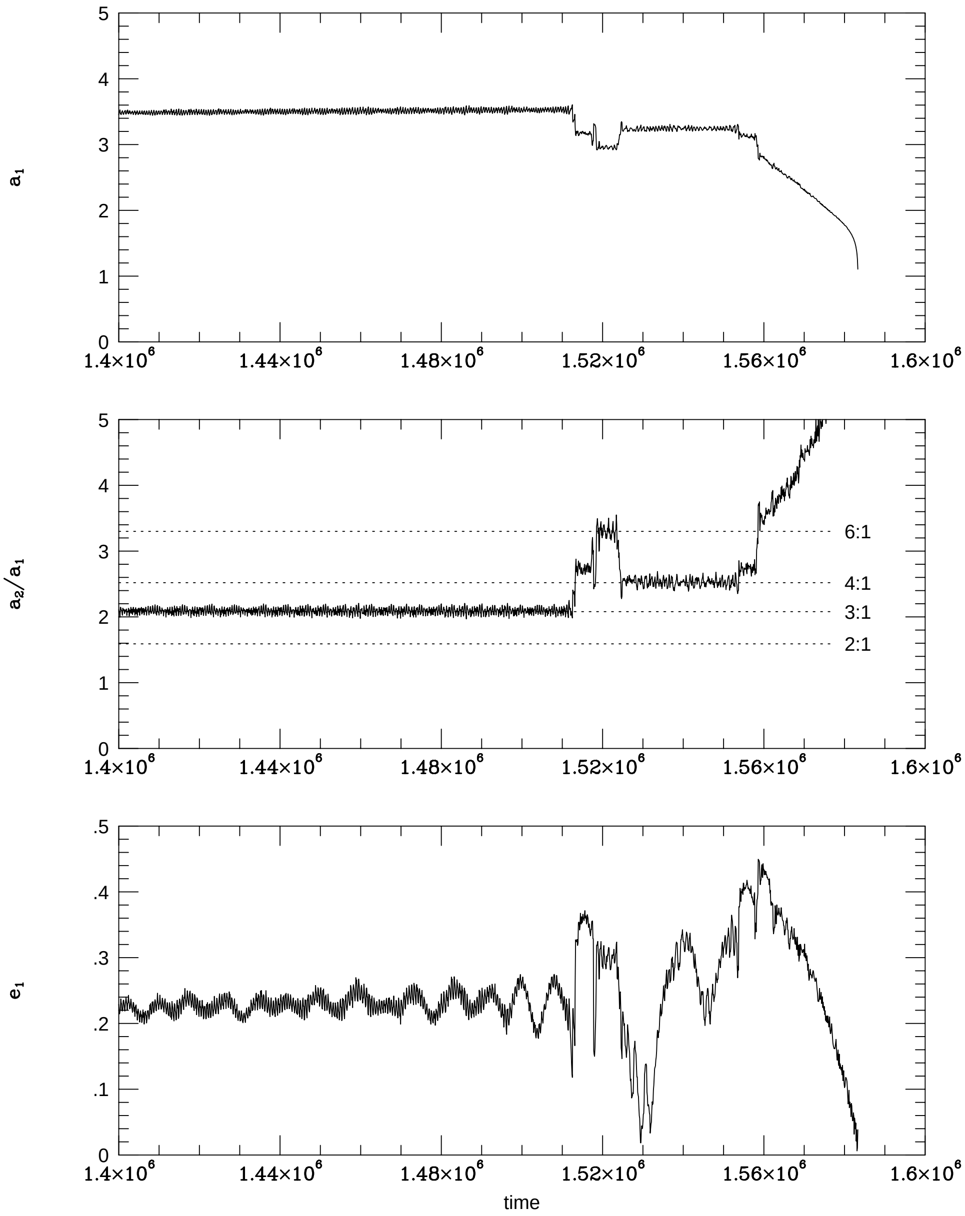

5
4
3
2
1
0
a1
1.4×10^6
1.44×10^6
1.48×10^6
1.52×10^6
1.56×10^6
1.6×10^6
a2/a1
6:1
4:1
3:1
2:1
.5
.4
.3
.2
.1
e1
time

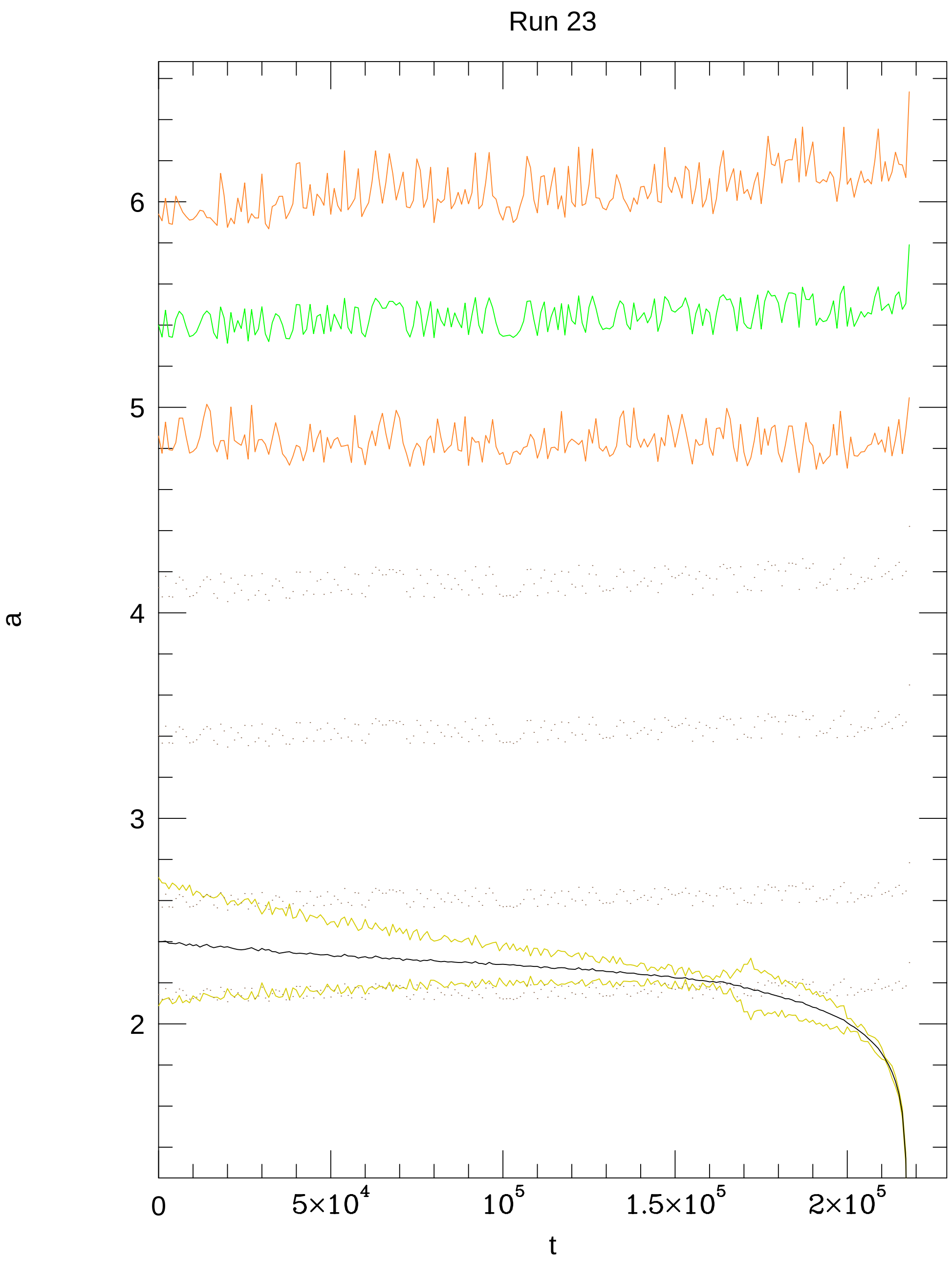

Fig. 6.— The evolution of another two-moon case from ICS97 (their Run 12). Here periapse of m_1 is initially inside synchronous orbit for a terrestrial day of 5 hours, and the inner moon collides with the Earth after about 5 years.

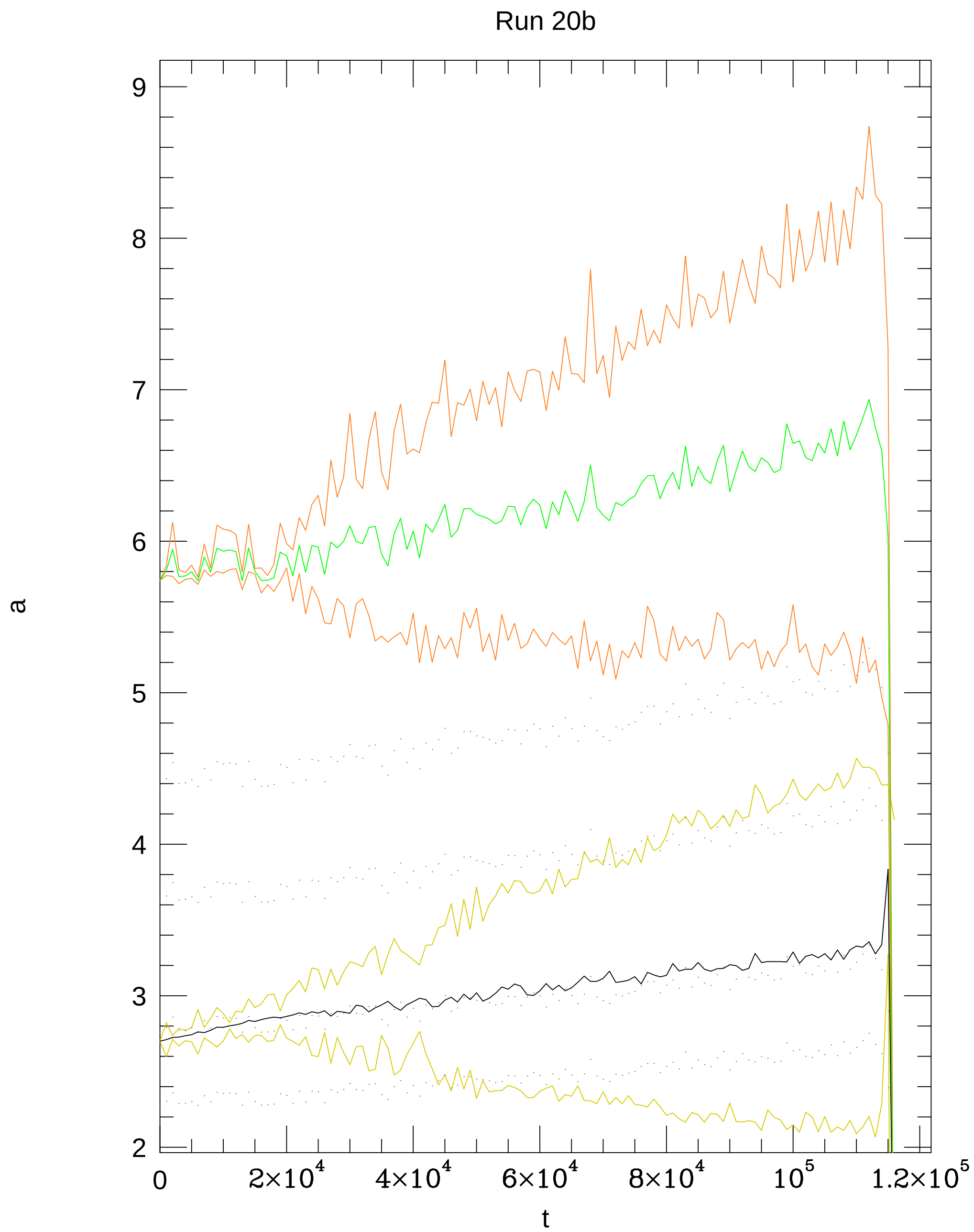

Fig. 7.— The evolution of same two-moon ICS97 case as shown in Figure 5, but here we have used a terrestrial day of 2.5 hours ($a_{sync} \sim 1.5R_{\oplus}$). The moons are again captured into the 3:1-e_1e_2 resonance, but in this case they experience a close encounter after about 3 years.

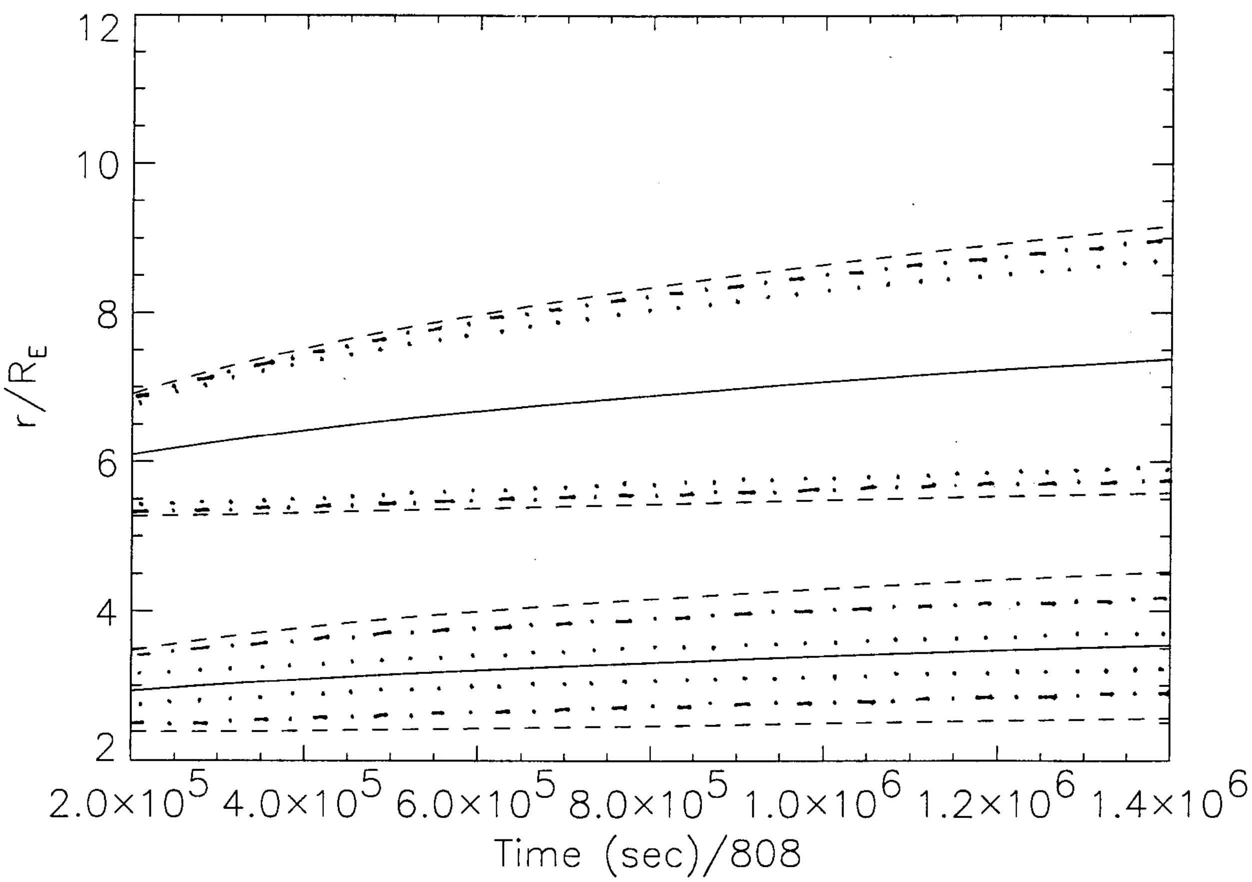

Fig. 8.— The anaytic predictions for the case shown in Figure 5 for A=0 (dashed), A=1 (dot-dashed) and A=10 (dotted). In this case, e_2 has an equilibrium eccentricity less than unity only for $A \gtrsim 1.5$.

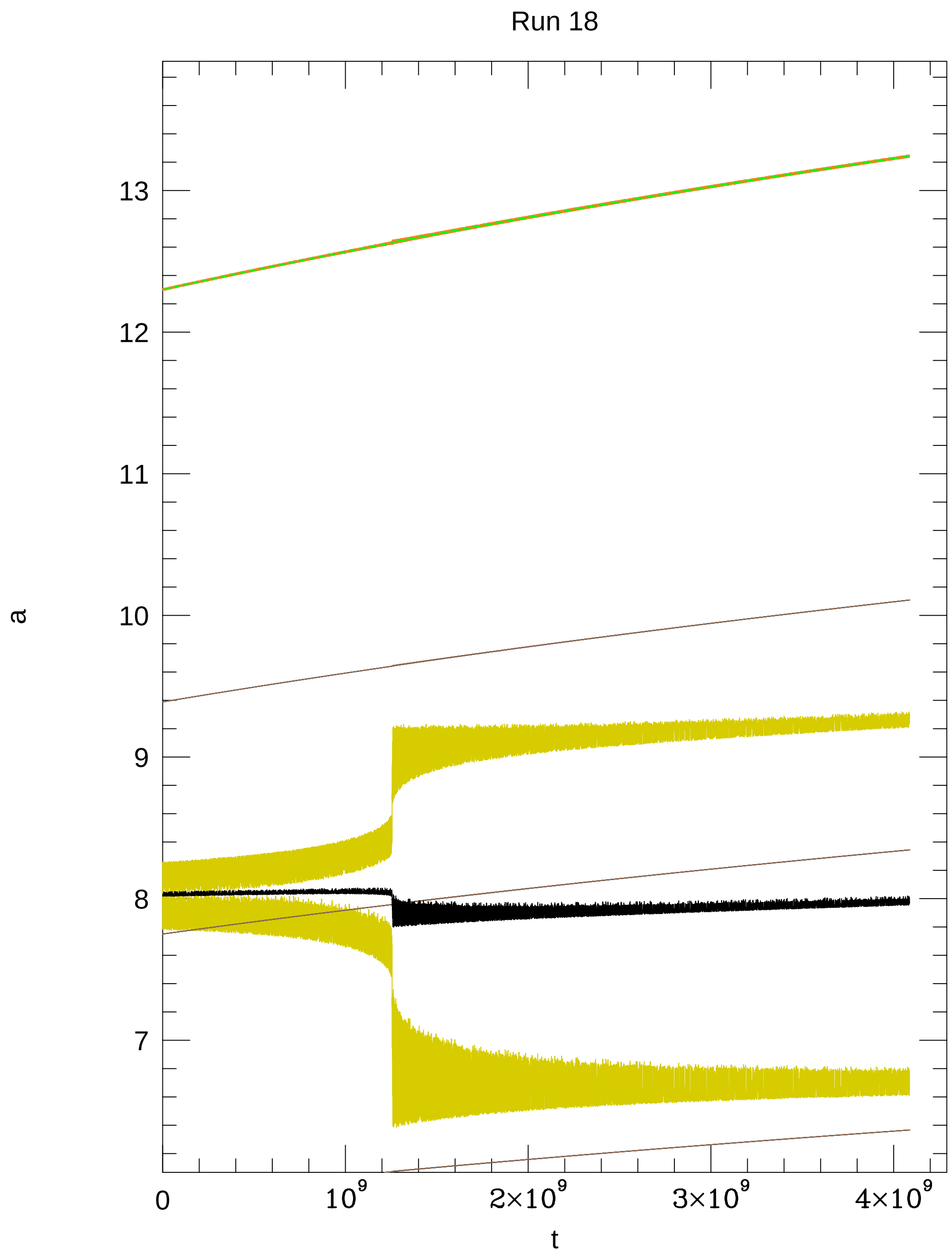

Fig. 9.— The evolution of two moonlets with $m_1, m_2 = 5 \times 10^{22}, 5 \times 10^{24}$ g. Here the moonlet orbits are diverging due to tides and so capture into resonance does not occur. The inner moonlet experiences a jump in eccentricity as it diverges through the 2:1-e_1 resonance.

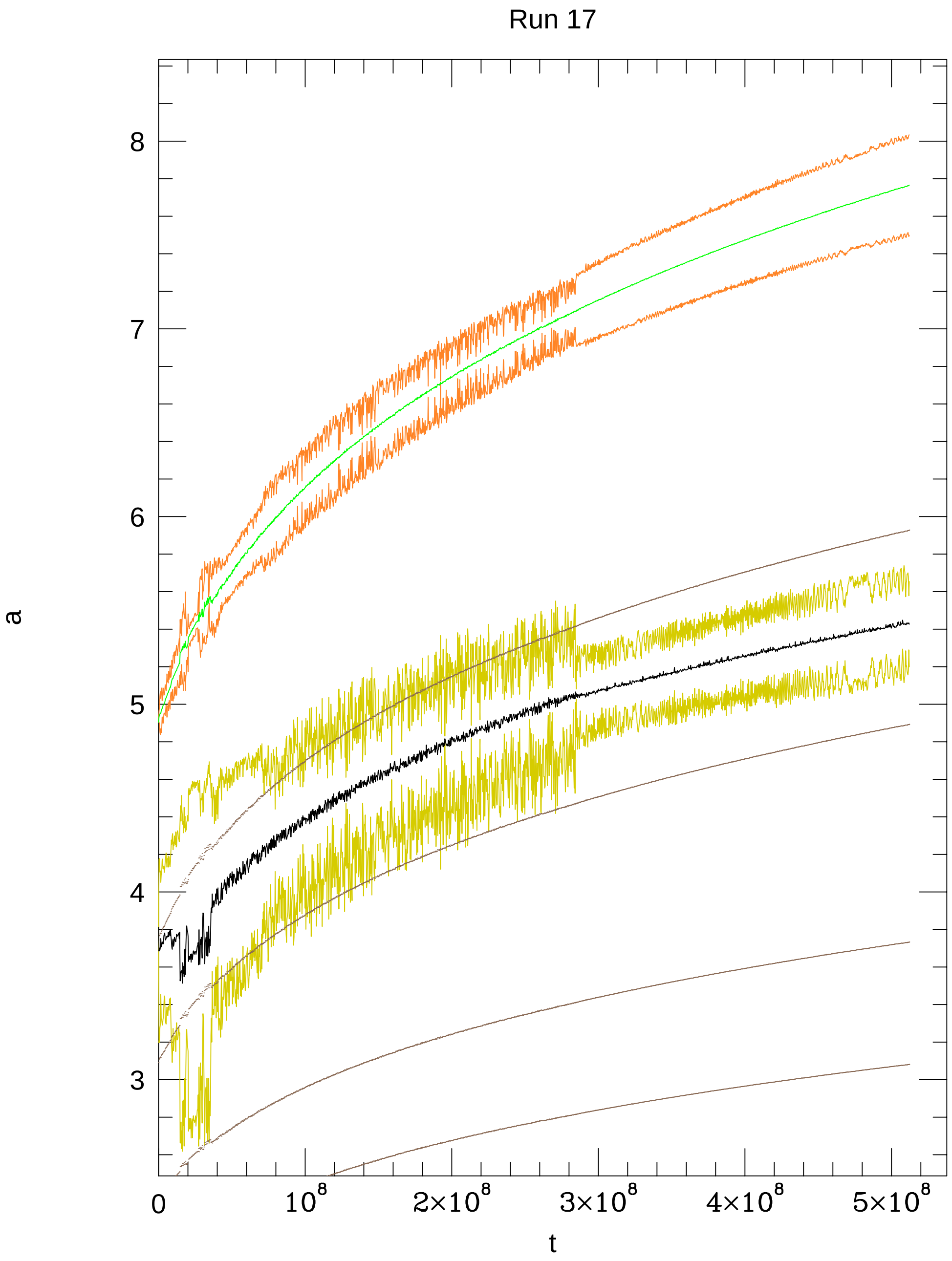

Fig. 10.— The evolution of two moonlets with $m_1, m_2 = 3.6 \times 10^{23}, 3.6 \times 10^{24}$ g. The moons are initially just outside the 3:2, and remain on diverging, potentially stable orbits at the end of the simulation.

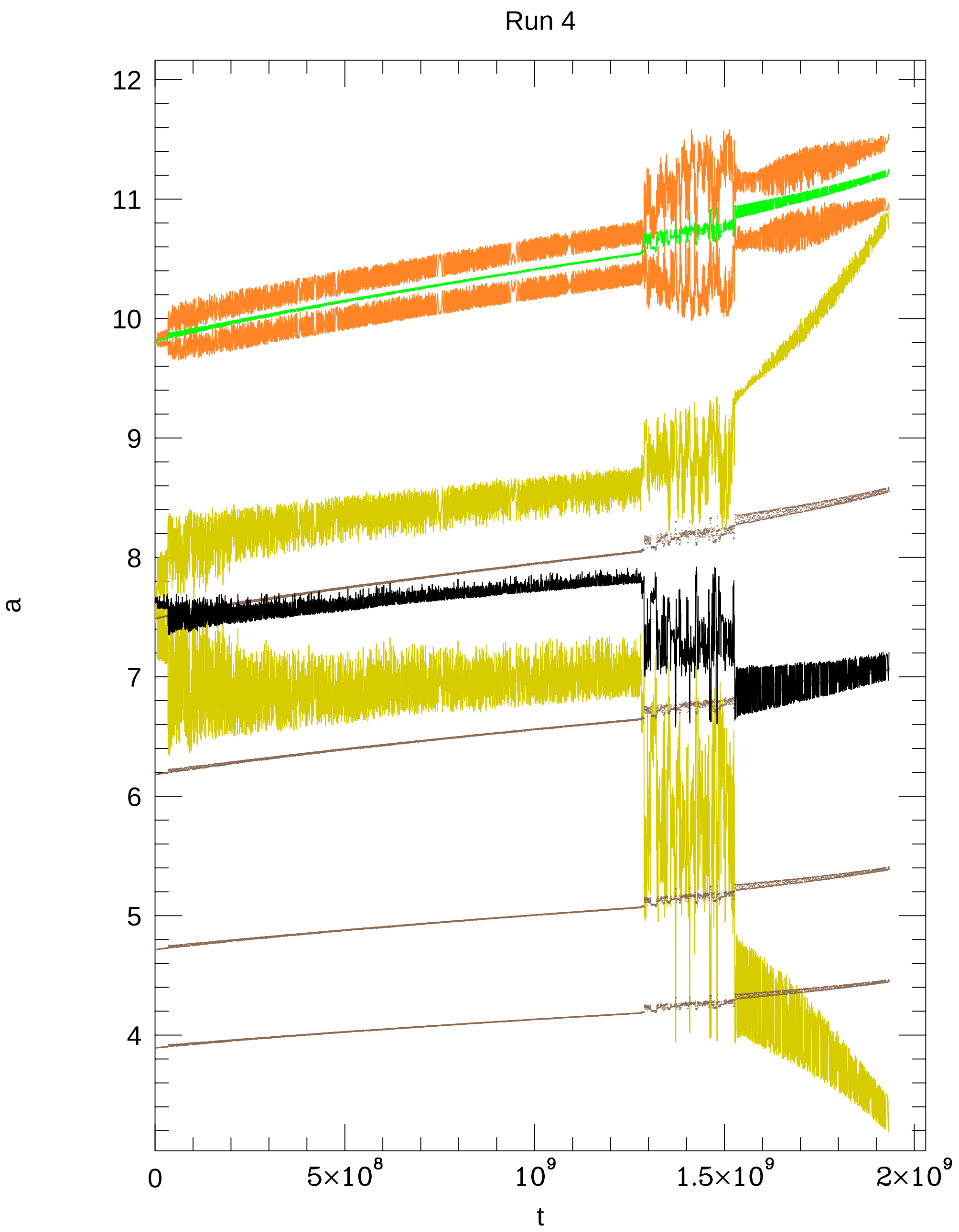

Fig. 11.— A simulation using the same m_1, m_2, and a_1/a_2 values as in Figure 10, only here the moons are initially farther away from the planet. In this case, capture into the 2:1 leads to orbit crossing.

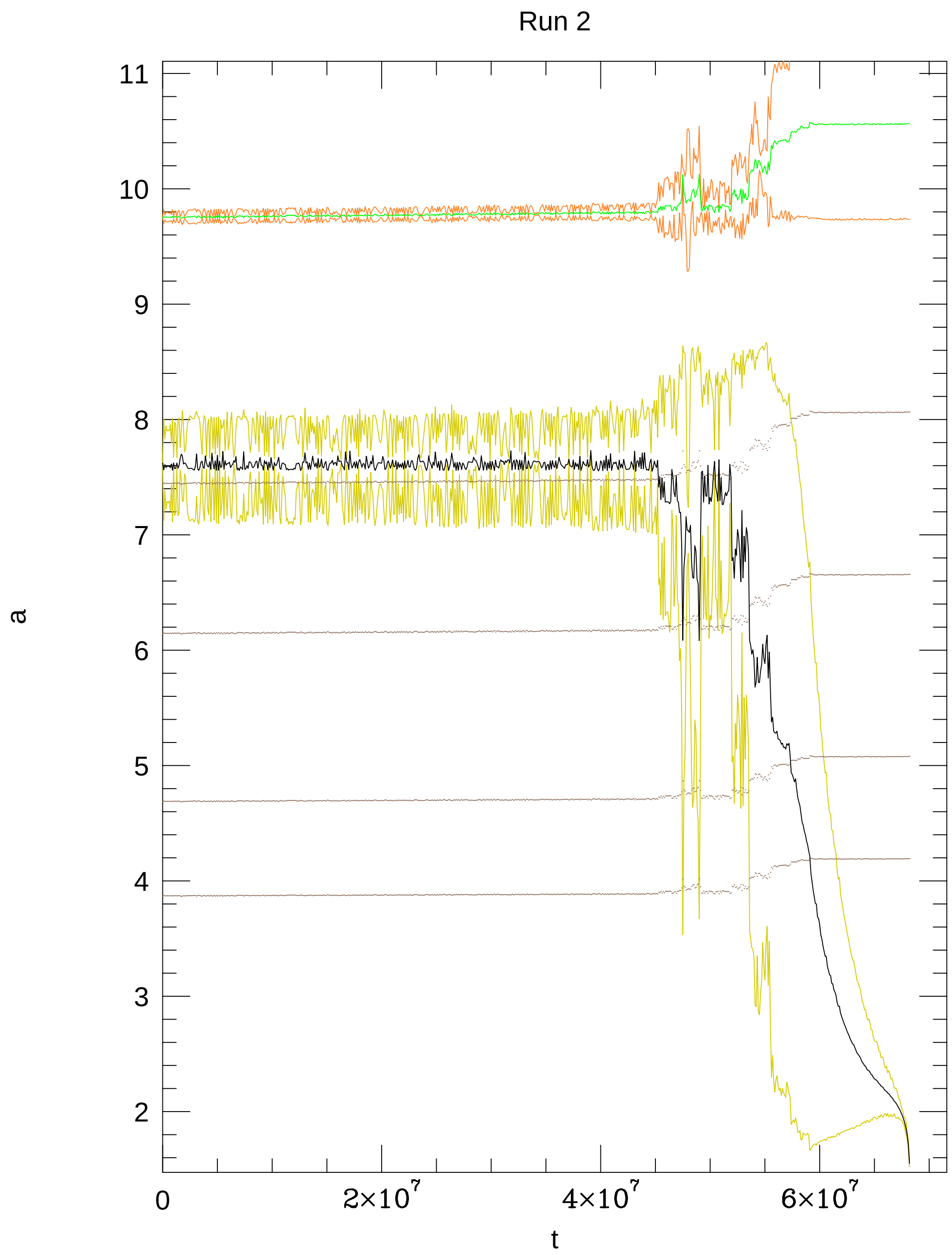

Fig. 12.— Numerical integration of two moons with $m_1, m_2 = 5 \times 10^{23}, 5 \times 10^{24}$ g. Jumps in e_1 eventually bring periapse of the inner moon to within synchronous orbit (about $2.3 R_\oplus$), where tides cause it to evolve inward and collide with the Earth after about 2060 years.